Grumman Research Department Report RE-571

TORNADO-TYPE WIND ENERGY SYSTEM

Technical Status Report
for period of
27 September 1976 to 28 February 1978

by

NATIONAL RENEWABLE ENERGY LABORATORY
LIBRARY

JAN 20 2005

GOLDEN, COLORADO 80401-3393

James T. Yen

Research Department
Grumman Aerospace Corporation
Bethpage, New York 11714

March 1979

Prepared for the

UNITED STATES DEPARTMENT OF ENERGY
DIVISION OF SOLAR ENERGY
WIND ENERGY SYSTEMS BRANCH
WASHINGTON, D.C. 20545

DoE CONTRACT NO: E(49-18)2555

Approved by: Richard A. Scheuing
Richard A. Scheuing
Director of Research

NWTC 990601

NOTICE

This report was prepared as an account of work sponsored by an agency of the United States Government. Neither the United States nor any agency thereof, nor any of their employees, makes any warranty, expressed or implied, or assumes any legal liability or responsibility for any third party's use or the results of such use of any information, apparatus, product or process disclosed in this report, or represents that its use by such third party would not infringe privately owned rights.

TABLE OF CONTENTS

Section		Page
	Executive Summary	xi
1	Introduction	1
2	Experimental Investigations	5
3	Flow Analysis	41
4	Structural and Cost Analysis	59
5	References	71

LIST OF ILLUSTRATIONS

Figure		Page
1	Artist's Conception of Tornado-Type Wind Energy System.	xii
2	Planform of Grumman Research Tunnel Laboratory.	6
3	Survey of Wind Speed Over a Cross-Section of the 1.2x1.8m Wind Tunnel; Averaging Time Constant = 10 sec; X and Y Denote Location of Individual Probes	7
4	Defining the Coordinates for the Spiral Cross-Section	8
5	Pressure Measurements on the Tower Bottom Wall with a Solid Plug or a 3.81 cm diameter Screen-Simulated Turbine (C_T = 4.77). Measurements are made along θ=0° and 180° as defined in Fig. 4. . .	9
6	Pressure Measurements on the Tower Bottom Wall with a Solid Plug or a 3.81 cm diameter Screen-Simulated Turbine (C_T = 4.77). Measurements are made along θ=90° and 270° as defined in Fig. 4 . .	10
7	Measured Pressure Distributions Along the Tower Walls for V_∞ = 55.5 m/s (124 mph) and H = 76cm (30 in.) (No Blower).	11
8	Measured Pressure Distributions Along Tower Walls for H = 66cm (26 in.).	12
9	Flow Visualization of the Vortex Core, with a Screen-Simulated Turbine	13
10	Flow Visualization of the Vortex Core, with a Bladed Turbine.	14
11	Theoretical Maximum Power Coefficient Based on Tower Frontal Area (From Ref. 6).	16
12	Theoretical Maximum Power Coefficient Based on Tower Frontal Area (From Ref. 7).	16
13	Tunnel Blockage Effect Due To An Airscrew (Ref. 8).	17
14	Experimental Setup with Screen-Simulated Turbine.	17
15	Photograph of Towers, Turbines and Generators Used in Tests	19

Figure		Page

16 Plot of Power Coefficient C_P versus Disk Loading Coefficient C_T for D = 12.7 cm (5 in.), H/D = 2 and Different D/D_{Turb} Ratios . . 21

17 Plot of Power Coefficient C_P versus Disk Loading Coefficient C_T for D = 12.7 cm (5 in.), H/D = 2.8 and Different D/D_{Turb} Ratios. 21

18 Plot of Power Coefficient C_P versus Disk Loading Coefficient C_T for D = 12.7 cm (5 in.), H/D = 4.2 and Different D/D_{Turb} Ratios. 22

19 Plot of Power Coefficient C_P versus Disk Loading Coefficient C_T for D = 12.7 cm (5 in.), D/D_{Turb} = 5 and Different H/D Ratios. . 22

20 Plot of Power Coefficient C_P versus Disk Loading Coefficient C_T for D = 12.7 cm (5 in.), D/D_{Turb} = 3.3 and Different H/D Ratios. 23

21 Plot of Power Coefficient C_P versus Disk Loading Coefficient C_T for D = 25.4 cm (10 in.), H/D = 2.1 and Different D/D_{Turb} Ratios 23

22 Plot of Power Coefficient C_P versus Disk Loading Coefficient C_T for D = 25.4 cm (10 in.), H/D = 4.2 and Different D/D_{Turb} Ratios 24

23 Plot of Power Coefficient C_P versus Disk Loading Coefficient C_T for D = 25.4 cm (10 in.), D/D_{Turb} = 5 and Different H/D Ratios . 24

24 Scaling Law, Plot of Power Coefficient C_P versus Reynolds Number Re for D/D_{Turb} = 3.3 and Different H/D Ratios 25

25 Scaling Law, Plot of Power Coefficient C_P versus Reynolds Number Re for D/D_{Turb} = 5 and Different H/D Ratios 25

26 Comparison of Data from 1.2 x 1.8 m (4x6Ft) Tunnel with Previous Data from .6 x .9 m (2x3 Ft) Tunnel with the Same Model 28

27 Experimental Setup with Bladed Turbine and Electrical Generator . . 28

28 Plot of Power Coefficient C_P versus Tip Speed Ratio X for D = 25.4 cm (10 in.), D/D_{Turb} = 2.5 and Different H/D Ratios. . . . 30

29 Plot of Measured Disk Loading Coefficient versus Tip Speed Ratio for the Cases of Figure 28. 30

30 Plot of Generator and Turbine Efficiencies versus Tip Speed Ratio for the Cases of Figure 28. 31

31 Plot of Power Coefficient C_P versus Tip Speed Ratio X for D = 25.4 cm (10 in.), D/D_{Turb} = 5 and Different H/D Ratios. 31

Figure		Page
32	Plot of Measured Disk Loading Coefficient versus Tip Speed Ratio for the Cases of Figure 31.	32
33	Plot of Power Coefficient C_P versus Tip Speed Ratio X for $C_T = 10$ and X = 2, $D/D_{Turb} = 5$ and Different H/D Ratios	32
34	Plot of Measured Disk Loading Coefficient versus Tip Speed Ratio for the Cases of Figure 33.	34
35	Variation of Wind Speed with Height, Exhibiting the Nocturnal Boundary-Layer Maxima	38
36	Variation of Wind Speed with Height, Exhibiting the Noon Time Boundary-Layer Maxima	38
37	Control Volumes and Nomenclature for Flow Analysis.	43
38	Inlet Flow Parameter (Alpha) versus Dimensionless Viscous Core.	49
39	Inlet Flow Parameter α vs Angle β	49
40	Accelerating Factor γ vs Inflow Parameter α	50
41	Schematic Representations of Flow Field Around Wind Energy Machines.	51
42	Static Pressure Distribution at Tower Bottom.	53
43	Plot of Power Coefficient versus Disk Loading Coefficient and Comparison of Theory and Experiment	55
44	Plot of Power Coefficient versus Disk Loading Coefficient for Various Values of D/D_{Turb}, H/D and δ/R.	57
45	Nomenclature for Structural Analysis.	60
46	Typical Pressure Distribution Around a Circular Cylinder (Ref. 16).	62
47	Plot of Specific Tower Cost Installed versus Tower Height for Different Materials and with 26.8 m/s (60 mph) Maximum Wind Speed	66
48	Plot of Specific Tower Cost Installed versus Tower Height for Different Materials and with 53.6 m/s (120 mph) Maximum Wind Speed	66

Figure		Page

49 Plot of Specific Tower Cost Installed versus Tower Height for Different Materials and with 71.5 m/s (160 mph) Maximum Wind Speed 67

50 Plot of Specific Tower Cost Installed versus Cost per Square Foot of Wall Area Installed for Different Scaling Laws and for a 300 m (1000 Ft) Tower Height. 67

EXECUTIVE SUMMARY

The Tornado-Type Wind Energy System is one of several advanced and innovative concepts being investigated under a DoE Wind Energy Program as potential ways to reduce the cost and broaden the usability of wind energy. This system (see Fig. 1) uses a large hollow tower to form an internal vortex, and the low pressure at the core of the tower provides an effective and low pressure exhaust reservoir for the turbine, which accepts a separate ram air inlet supply. The tower serves as a stationary and omnidirectional collector and concentrator capable of collecting large amounts of wind energy and concentrating the collected energy into a high power density turbine. This system combines the unique advantages of a compact, vertical-axis, enclosed, high efficiency turbine with a stationary, omnidirectional, and modularized tower. The components of the modularized tower can be mass produced on assembly lines, subassembled in the factory, and stacked in the field, thus providing for low-cost manufacturing, construction, and maintenance. These advantages also provide for fast delivery and an early return on investment. This wind energy system promises a structurally rugged and stable design for both land-based and offshore installations. Based on this design, large and low-cost multimegawatt wind energy systems may be developed and constructed for the utilities, and small and economically competitive systems may be provided for individual farms and homes. We hope that this system will make it possible to bring out fully the immense potential of wind energy.

This report presents the results of work carried out under contract E(49-18) - 2555 over a 17-month period from October 1976 to March 1978. Experimental results on the system performance with screen-simulated and simple bladed turbines are presented, followed by results from a flow analysis and a structural and cost analysis. Highlights of the results are as follows:

- Detailed pressure surveys on the tower bottom wall with screen-simulated turbines and small towers indicate that overall, the vortex is strengthened by the presence of the turbine as compared with the case when the tower has a solid bottom. (Pages 9 and 10.)

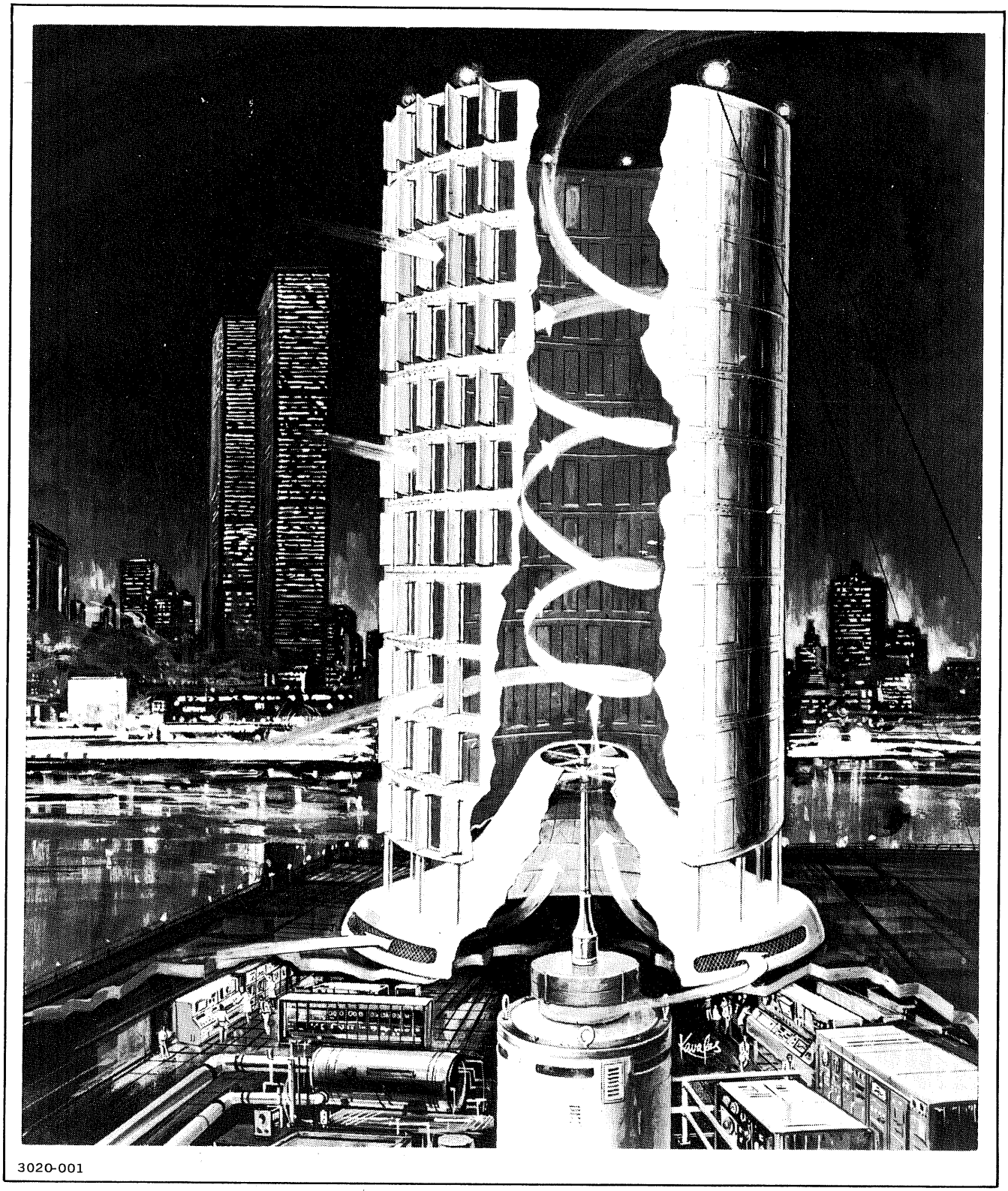

3020-001

Fig. 1 Artist's Conception of Tornado-Type Wind Energy System

- Flow visualization photos with smoke show well-confined vortex cores with some axial contraction and a further strengthening of the vortex when a bladed turbine replaces a screen-simulated turbine. The observed confinement of the vortex core is related to the favorable axial pressure gradient measured previously. Both observations are used to convey the conclusion that "vortex breakdown" does not occur within the tower. (Pages 12 and 14.)

- For the power coefficient based on the tower frontal area, there is no definite "Betz Limit" for aerodynamically augmented systems such as the Tornado tower, at least from theoretical considerations. This point is supported by results of some recent analyses. (Pages 16, 41-56.)

- Some discussions on the wind tunnel blockage effect are presented with the indication that the blockage effects on smaller models should be moderate, but not excessive for the purpose of determining performance levels and configuration trends. (Page 17.)

- Data on the power coefficient for screen-simulated and for simple bladed turbines with various tower geometries are presented. Best performance of 6.51 for the power coefficient based on the turbine area is obtained with a tall tower, and 0.18 for the power coefficient based on the tower frontal area is obtained with a short tower with a bladed turbine. (Pages 26 and 33, respectively.)

- Scaling laws are obtained from small-scale data that show a strong improvement of performance with tower size. Power coefficient varies with Reynolds number to a power ranging from 0.86 to 1.56. This is a much faster growth than the usual power of 0.2 to 0.3. (Page 25.)

- Based on the best value of 0.18 for the power coefficient measured with our small models, and assuming a conservative "average" exponential of 0.2 to 0.33 for the entire range between our small model and a full-scale system, it is found that the power output may exceed 100 to 200 MW with a reasonably sized tower, with a spiral cross section that has around 25% of its frontal area opened to the wind. There is some basis for the hope that multiple inlet vanes will allow greater performance when optimum configurations have been determined. (Pages 35-39.)

- A structural and cost analysis of a variable thickness tower shows that for tower heights up to around 300 m (1000 Ft), specific tower costs should remain below $160 per square meter ($15 per square foot) of tower surface area installed, for solid tower walls made of either ABS plastics, aluminum alloy, or steel; and with maximum wind speeds of 72 m/s (160 mph). (Pages 59-69.)

- Cost analysis applied to the above-mentioned full-scale system yields a system cost of less than $500/kWe installed and an energy cost of less than 2.7 cents/kWh. These costs are then compared with those for the propeller type Mod-OA and Mod-1 wind turbines. (Page 68.)

- Discrepancies between our present results and our previous data taken with the same small model in a smaller wind tunnel are discussed, including the finding that by enclosing the entire system within the wind tunnel, a large fraction of this discrepancy may be removed. (Page 28.)

- A discussion on the difficulties of model turbine design due to limitations imposed by the small sizes and small chord Reynolds numbers of our turbine blades is presented. Even with such crude turbines, however, good results are obtained and presented, including good power coefficients and good agreements between the measured and the design values of the turbine disk loading coefficient and of the tip-speed-ratio. (Page 29.)

- A flow analysis based on global or overall mass, momentum, and angular momentum balances is presented. Various parameters related to the inlet flow conditions, the flow state at the top exit of the tower, and the dimensions of the vortex core are included. Various findings are presented and discussed including the possibility of the acceleration of the incoming wind stream before it enters the tower, the deduction that the power coefficient improves strongly with the tower size or Reynolds number, and some realistic results on the dependence of the power coefficient versus the turbine disk loading. In spite of the simplicity of the global model, it is capable of tracking the essential physics of the problem and, in addition, gives us further insight into the mechanics of the system. (Page 41 ff.)

- Another effort to solve the mean turbulent momentum equations using an integral method and based on a generalized eddy viscosity for curved flows is briefly described, indicating the sensitivity of the results on the shapes of the assumed velocity profiles and that major modifications of the model are needed before we can obtain reliable results. (Page 41 ff.)

1. INTRODUCTION

The Tornado-Type Wind Energy System (Fig. 1) was first proposed in 1975 (Ref. 1). Detailed descriptions and some analyses of the system have been presented in Refs. 2 and 3. Since October 1976, investigations on this system have been carried out under the sponsorship of the U.S. Department of Energy. A semi-annual status report (Ref. 4) was issued in September 1977. The present report will sumamrize the results of Ref. 4 and present the progress made since September 1977.

This report is subdivided into four sections. A brief description of the Tornado-Type Wind Energy System and an outline of the goals of this investigation are presented below, followed by a summary of Sections 2, 3, and 4.

BRIEF DESCRIPTION OF THE SYSTEM

Tornado wind energy systems (TWES) use the core of a vortex to provide a low pressure exhaust reservoir for a wind turbine. The vortex is formed by the wind entering a hollow tower through a tangential inlet system, and exhausting out of the open top of the tower. The turbine is located at the bottom of the tower so that it can receive ram air from the wind and exhaust into the vortex center. The high turbine pressure differential made possible by this concept allows the use of a compact and high energy-density turbine. Many advantages of this arrangement have been discussed previously (Refs. 2 and 3) but their realization depends on satisfactory solutions to a number of technical problems. This report describes the first stages in the solution of these challenging problems.

The goals of the current effort are to determine:

- That the turbine in a TWES can produce many times the energy of a conventional wind turbine of the same diameter in the same wind
- That the power coefficient based on frontal area of the tower can be high enough such that with reasonable tower costs, the cost of energy from the TWES can be attractive

- Whether the usable pressure reduction with turbine flow into the vortex increases with the size (i.e., Reynolds number) of the entire system, so that higher performance in large units is a realistic expectation
- The configurations that produce best performance under different circumstances, and as much as possible the flow mechanisms responsible for the behavior of the device.

The air flows associated with the TWES are extremely complex, and no general method exists that can answer the various questions posed by the desire for optimum tower configuration, inlet designs, disk loading optimization, wake pressure recovery, vortex stability, etc. The following sections of this report show how we attacked these and related problems, and why we believe that the TWES will prove to be an extremely effective energy resource.

SUMMARY OF SECTIONS 2 TO 4

In Section 2, experimental results are presented. The wind tunnel velocity distribution is first shown, together with a sketch of the wind tunnel laboratory setup. Panels are used to reduce the previously measured nonuniformity of wind velocity within the tunnel. Data and observations on some favorable interactions between the vortex and turbine, and between the tower and vortex are discussed next, together with the implications of favorable axial pressure gradients and of the prevention of "vortex breakdown" within the tower.

The important point that theoretically there is no "Betz Limit" on the power coefficient based on the tower frontal area is then emphasized and supported with results of some recent analyses. Some discussions on wind tunnel blockage effect is presented.

Data on the power coefficient C_P for various screen-simulated turbines and various tower geometries are presented next, giving also the best values of C_P based on both tower frontal area and turbine area with the optimal value of the trubine disk loading coefficient, C_T, for these cases. The data are then summarized as scaling laws for the system performance, showing a strong improvement of performance with tower size.

A large discrepancy between the present results and our previous data taken with the same model in a smaller wind tunnel is then discussed, including the finding that by enclosing the entire system within the new tunnel, a large fraction of this discrepancy may be removed. The completion of this investigation will have to wait for the next contract phase.

A discussion follows on the difficulties of our turbine design, due to limitations imposed by the small sizes and small chord Reynolds numbers of the turbine blades. Even with such crude turbines, however, good results are obtained and discussed next, including good power coefficients and good agreement between the measured and the design values of the turbine disk loading coefficient and tip-speed-ratio.

The best experimental performance of $C_P = 0.18$ based on the tower frontal area for a short tower with $H/D = 2.1$, $D/D_{Turb} = 2.5$ and $D_{Turb} = 10$ cm (4 in.) is then combined with a conservative scaling law of $C_P \sim Re^m$ with $m = 0.3$ to 0.4 to give a prediction of power output of a full scale system. It is found that the power output may exceed 100 to 200 MW with a reasonably sized tower, even with a spiral cross-section, i.e., with only around 25% of its frontal area opened to the wind. Data were also gathered on one multivaned tower. Reduction of these data will be completed and reported later.

In Section 3, results on our flow analysis are presented based on a global or overall analysis. The analysis includes mass, momentum, and angular momentum balances taken over the tower and incorporates various parameters related to the inlet flow conditions, the flow state at the top exit of the tower, and the dimensions of the viscous vortex core. Various findings are presented and discussed including the possibility of the acceleration of the wind stream before it enters the tower, the deduction that the power coefficient improves strongly with the tower size or Reynolds number, and some realistic results on the dependence of the power coefficient versus the turbine disk loading. In spite of the simplicity of the global model, it is capable of tracking the essential physics of the problem and in addition, gives us further insight into the mechanics of the system.

An effort to solve the mean turbulent momentum equations using an integral method and based on a generalized eddy viscosity for curved flows is briefly described, indicating the sensitivity of the results on the shape of the

assumed velocity profiles. Major modifications of the model are needed before we can obtain reliable results.

A structural and cost analysis of a variable wall thickness vortex tower is presented in Section 4, using a method based on the principle of linear superpositions and including a realistic wind loading distribution. Results are presented and discussed, indicating that for tower heights up to around 300 m (1000 Ft), specific tower cost remains below $160 per square meter ($15 per square foot) of tower surface installed and is relatively constant, i.e., it is principally determined by the tower weight and is rather independent of the wind speed up to 72 m/s (160 mph). For shorter towers, ABS plastic is the cheaper material to use, although for large towers, steel proves to be the most economic structural material. It is pointed out that since the tower cost is principally determined by the tower weight, utilization of sandwich and lightweight materials may further reduce the tower costs.

Specific tower cost per kWe installed is then computed to yield a value of $125 to 330/kWe installed for a tower of 300 m (1000 Ft) in height, 150 m (500 Ft) in diameter with a 61 m (200 Ft) diameter turbine rated at a wind speed of 11 m/s at 9 m (25 mph at 30 Ft). This system, which is estimated to have a rated output of 90 to 190 MWe based on a conservative scaling law, is estimated to have a mass production system cost of less than $500/kWe installed and an energy cost of less than 2.7 cents/kWh. These costs are then compared with those for the propeller-type Mod-OA and Mod-1 wind turbines.

2. EXPERIMENTAL INVESTIGATIONS

The main facility for our investigation is a new 1.2 x 1.8 m (4 x 6 Ft) low speed wind tunnel. A major effort, which was outside the scope of this contract, involved the design and construction of the tunnel and smoothing of the flow velocities in it. Since the size of the laboratory return path is not sufficient to settle the exhaust from the wind tunnel to low levels of fluctuations before it re-enters the tunnel, large fluctuations were initially present within the tunnel. This nonuniformity would lead to an unacceptably large uncertainty in the power coefficient, as mentioned in Ref. 4. Following an extensive effort described in Ref. 4, the spatial nonuniformity of the tunnel wind speed was reduced (see Fig. 8 of Ref. 4). Since then, an additional effort was made aimed at a significant further reduction of the nonuniformity particularly within the lower portion of the wind tunnel. A planform of our wind tunnel laboratory is sketched in Fig. 2 showing the panels used to reduce the non-uniformity. The improved uniformity of the velocity is shown in Fig. 3 where the overall scatter of the velocity data has been reduced to 3.7% from the previous 7%. The experimental investigation in the 1.2 x 1.8 m (4 x 6 Ft) wind tunnel was initiated on September 16, 1977.

Prior to the completion of this wind tunnel, models of 0.36 m (14 in.) in height and 0.13 m (5 in.) in diameter with spiral-shaped cross sections (Fig. 4) were tested first in a smaller 0.6 x 0.9 m (2 x 3 Ft) wind tunnel at a 5.8 m/s (12.8 mph) wind speed. Detailed static pressure surveys were made on the tower bottom. The aim was to find out if the vortex pressure distribution is significantly weakened due to the presence of a turbine which exhausts into the core of the vortex. Typical results have been presented as Figs. 3 and 4 of Ref. 3 which are reproduced here as Figs. 5 and 6. Static pressure surveys were made on the tower bottom for two cases: first, with the vortex alone in a tower having a solid bottom, and second, with the vortex and a turbine exhausting into its core. Figures 5 and 6 show that most of the static pressure readings are reduced with the introduction of the turbine which is simulated here by a set of screens. Since a further reduction in the static pressure means a strengthening of the vortex, it is concluded in Ref. 3 that overall, the vortex is strengthened by the presence of the turbine. The reasoning is that with the vortex alone, it is

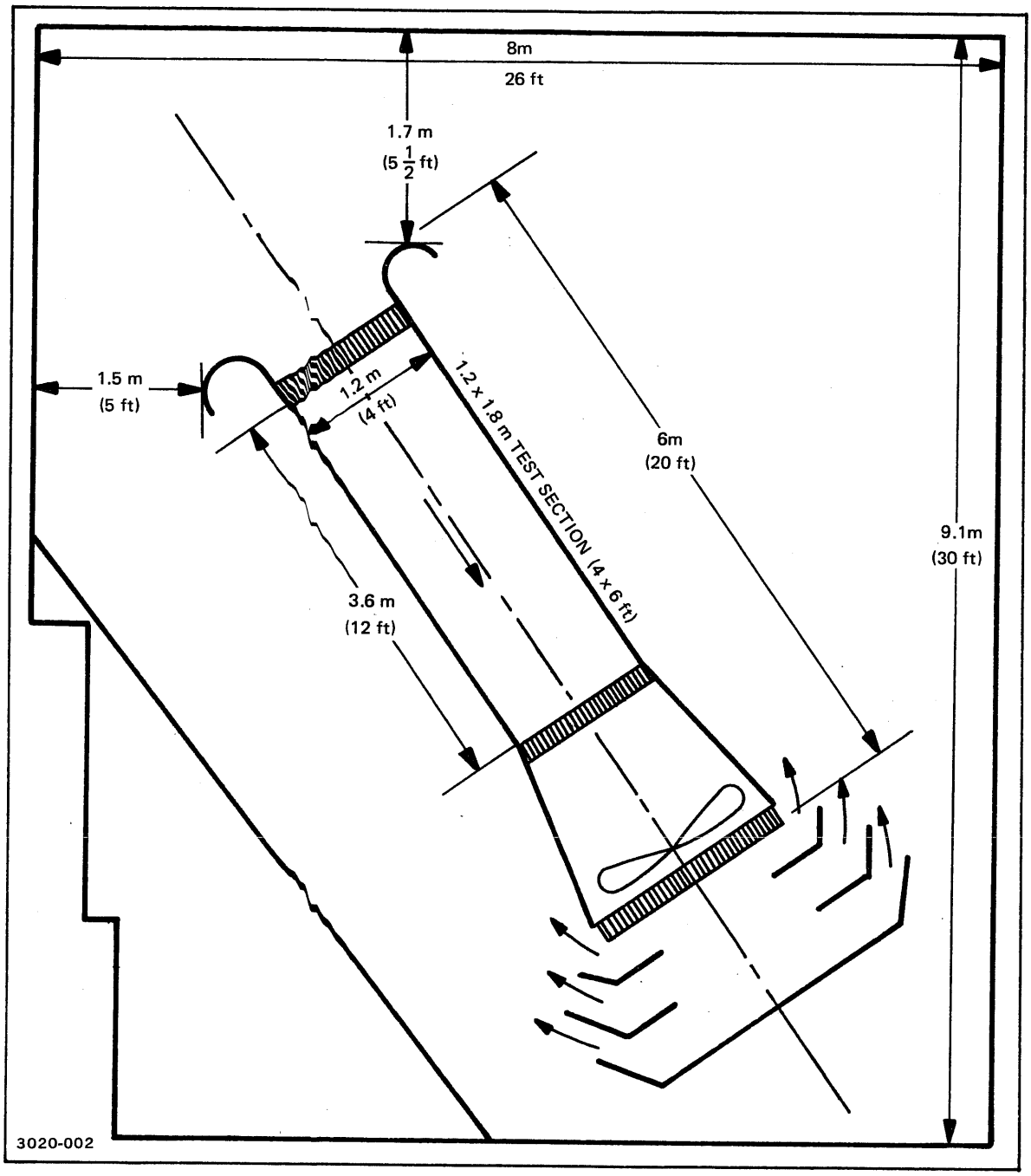

Fig. 2 Planform of Grumman Research Tunnel Laboratory

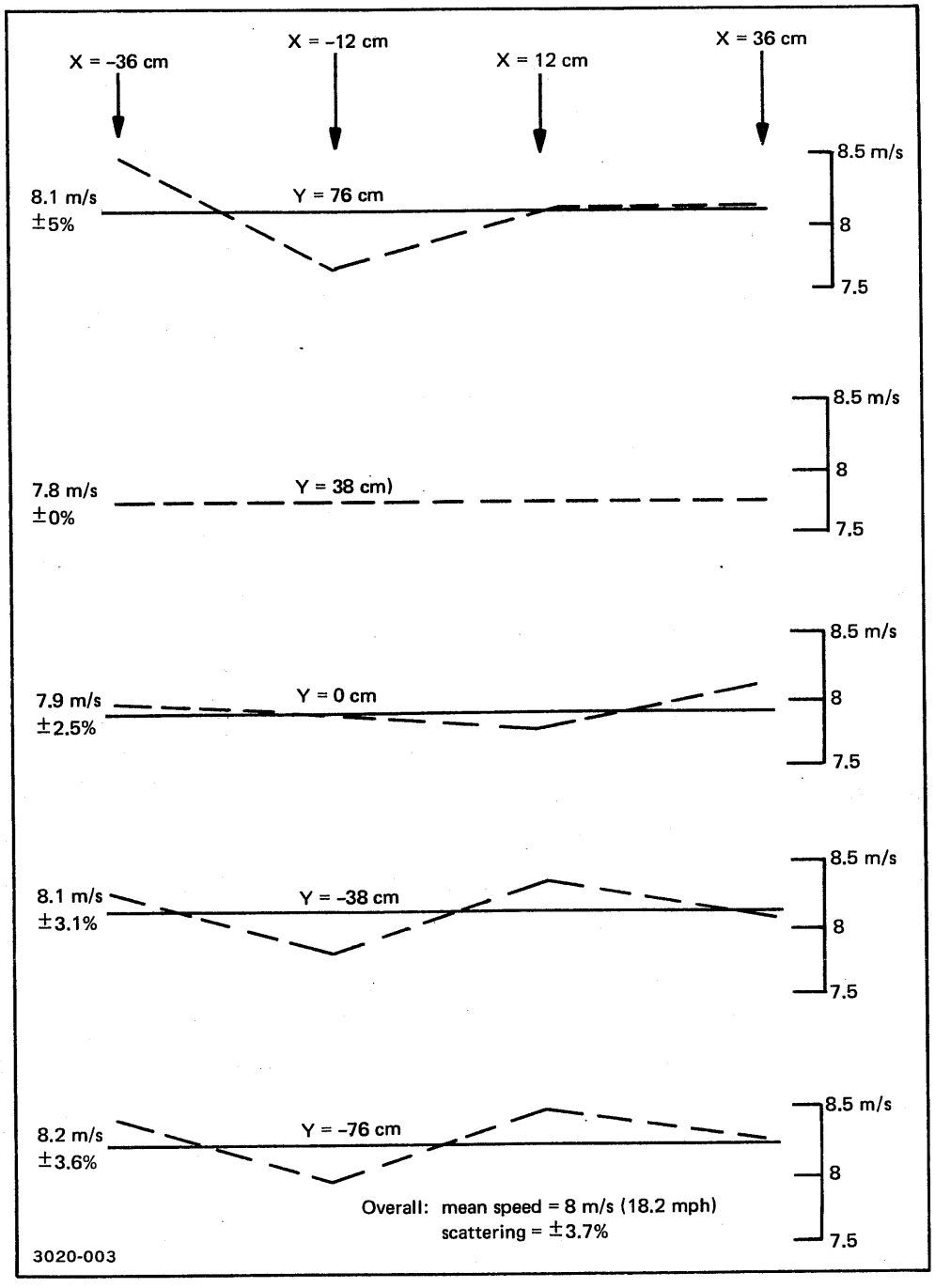

Fig. 3 Survey of Wind Speed Over a Cross-Section of the 1.2 x 1.8m Wind Tunnel; Averaging Time Constant = 10 sec; X, Y Denote Location of Individual Probes

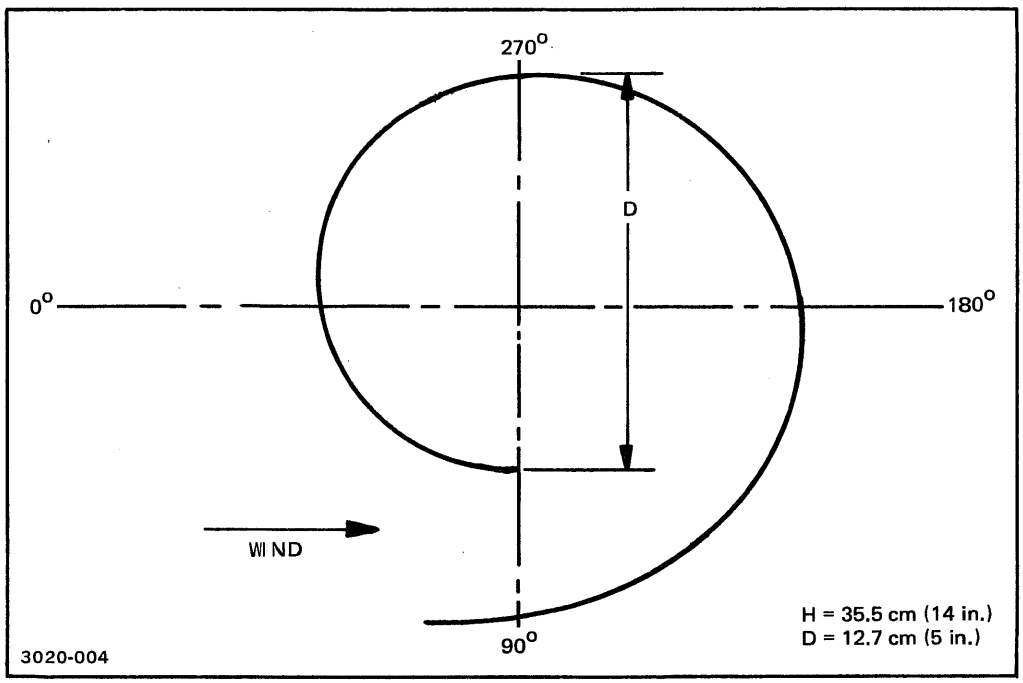

Fig. 4 Defining the Coordinates for the Spiral Cross Section

bounded by a solid bottom. Due to the viscous effect, high vortex tangential velocities set up large velocity gradients and high viscous stresses particularly over the central portion of the solid bottom wall which lies directly below the vortex core. When this portion of the solid bottom wall is removed and replaced by a turbine, the viscous loading on the vortex is reduced and the vortex strengthened. Also, it is well known (Ref. 5) that a vortex can be strengthened by injecting a flow into its core if the flow is in the forward direction of the vortex axial velocity. Such is the case for our turbine exhaust and this interaction may further strengthen the vortex axial velocity. Summarizing, it is seen that the vortex is not weakened but rather strengthened when the turbine is installed to exhaust into the core of the vortex.

Another interaction between the vortex and the collecting tower is also beneficial as mentioned in Ref. 2. This interaction results in setting up a decreasing or favorable axial pressure gradient within the tower as seen in Figs. 7 and 8. This favorable pressure gradient prevents the occurrence of "vortex breakdown" and keeps the vortex intact and strong within the tower. Kerosene vapor is used in Figs. 9 and 10 to visualize this effect. The vapor

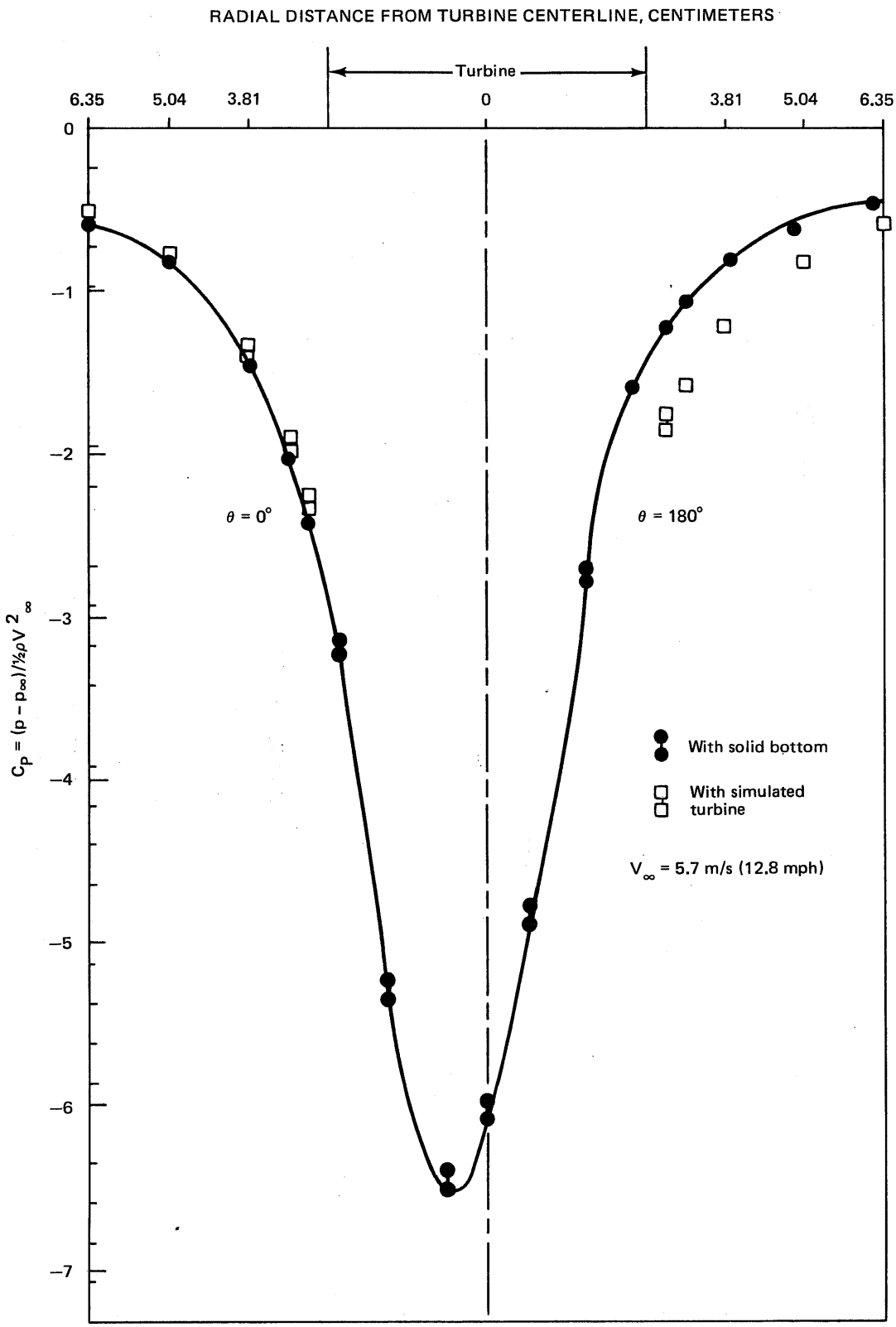

Fig. 5 Pressure Measurements on the Tower Bottom Wall with a Solid Plug or a 3.81 cm-diameter Screen-Simulated Turbine (C_T = 4.77). Measurements are made along $\theta = 0^o$ and 180° as defined in Fig. 4.

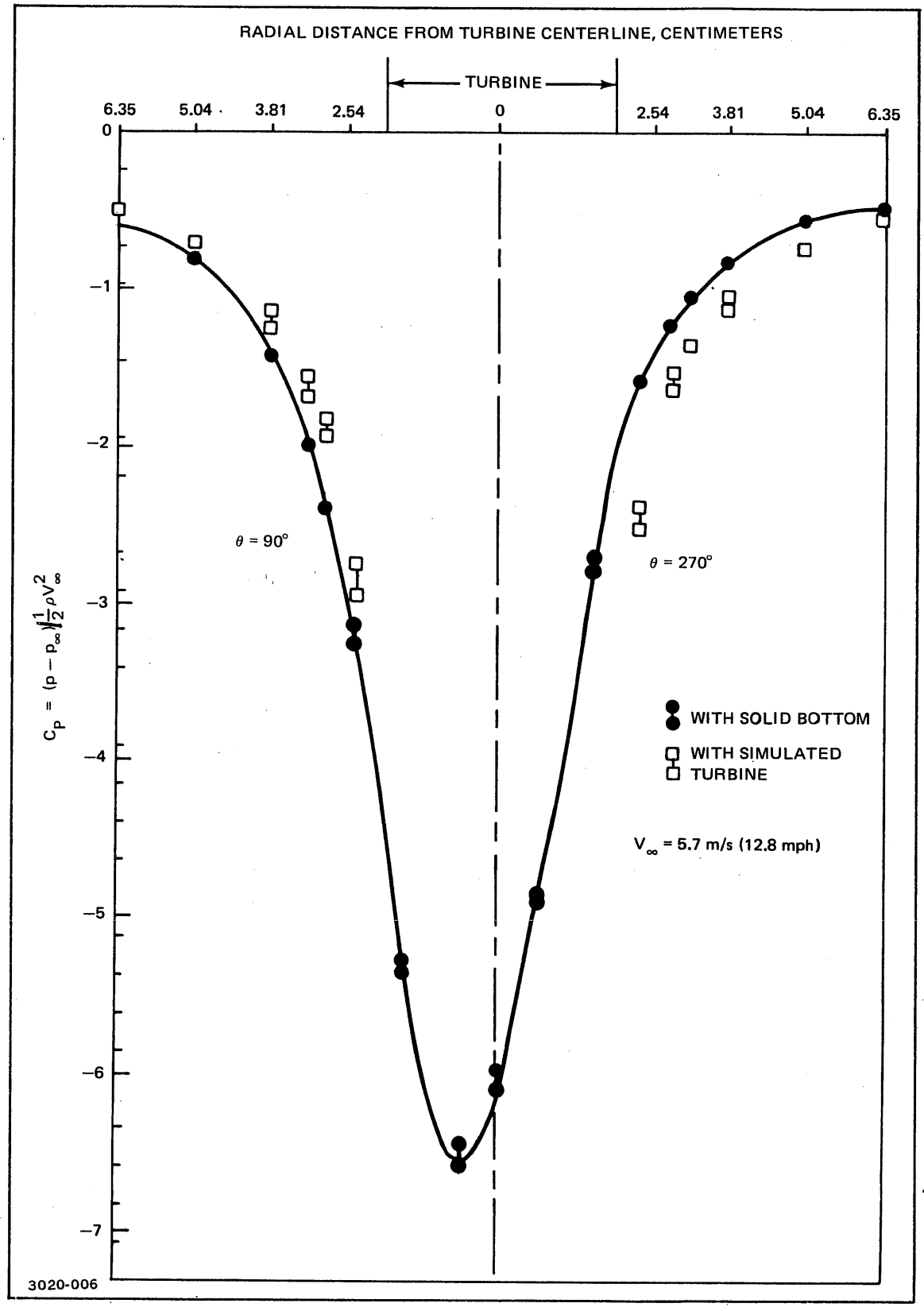

Fig. 6 Pressure Measurements on the Tower Bottom Wall with a Solid Plug or a 3.81 cm-diameter Screen-Simulated Turbine (C_T = 4.77). Measurements are made along θ = 90° and 270° as defined in Fig. 4.

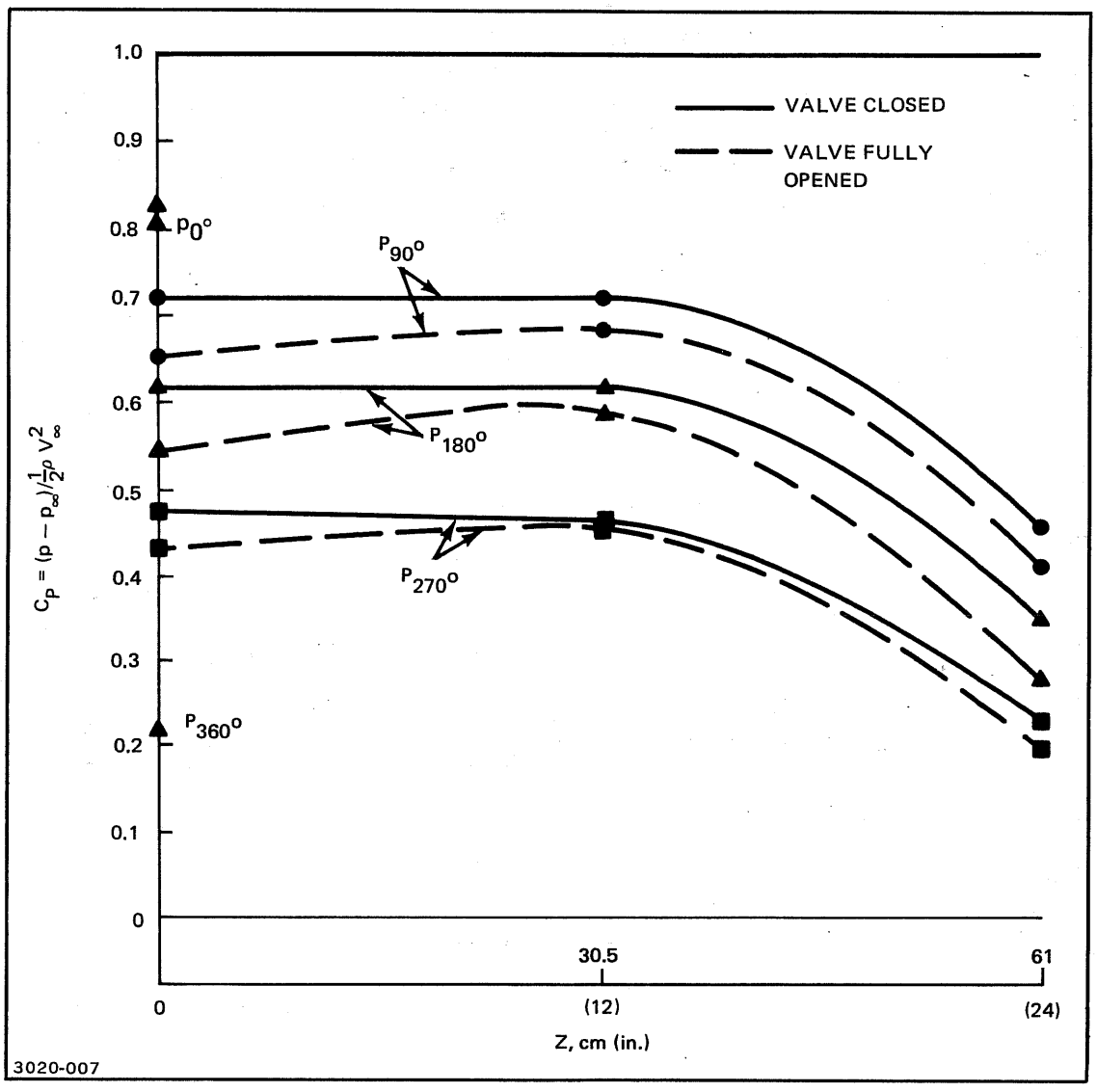

Fig. 7 Measured Pressure Distributuions along the Tower Walls for V_∞ = 55.5 m/s (124 mph), and H = 76 cm (30 in.). (No blower)

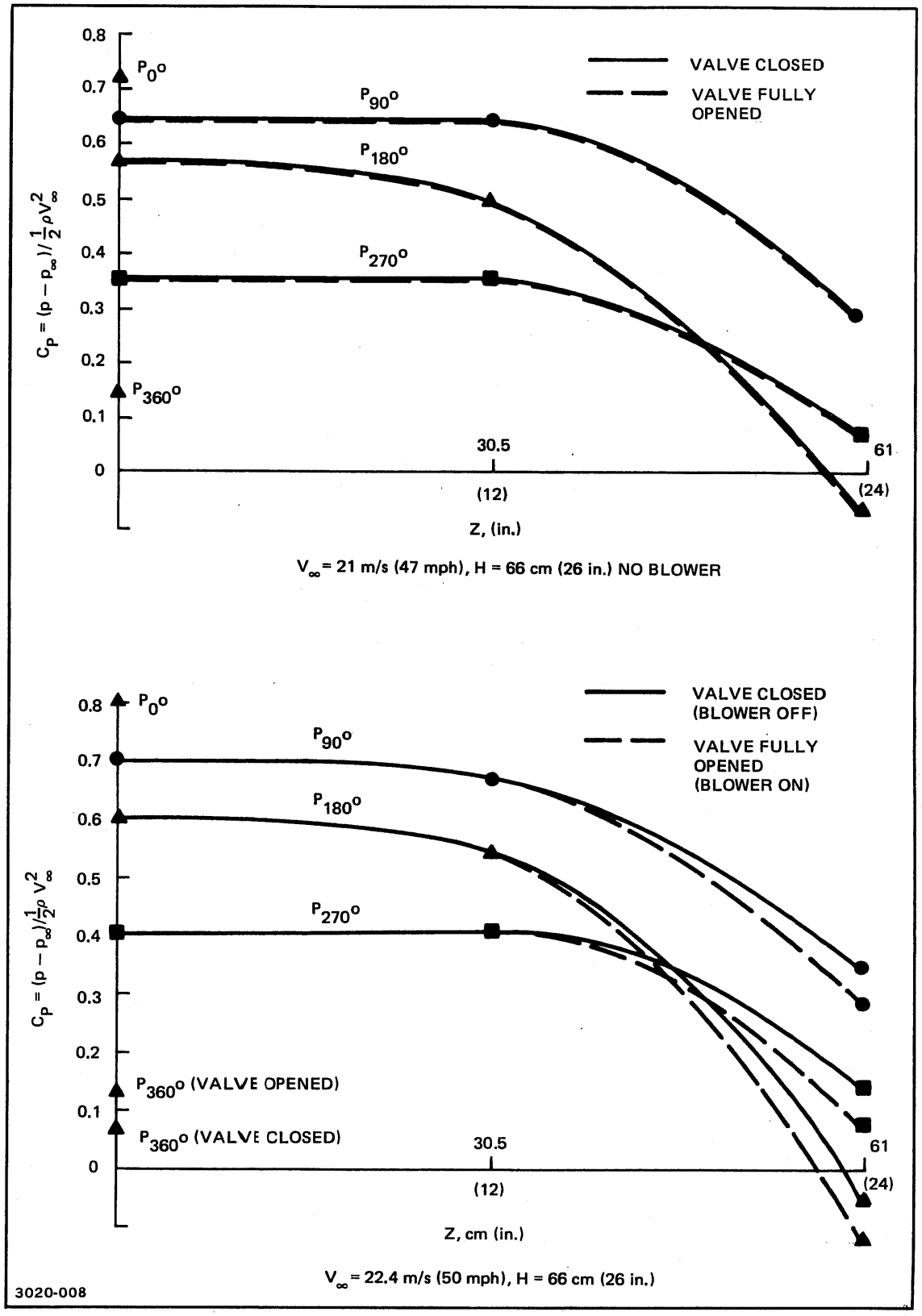

Fig. 8 Measured Pressure Distributions Along Tower Walls for H = 66 cm (26 in.)

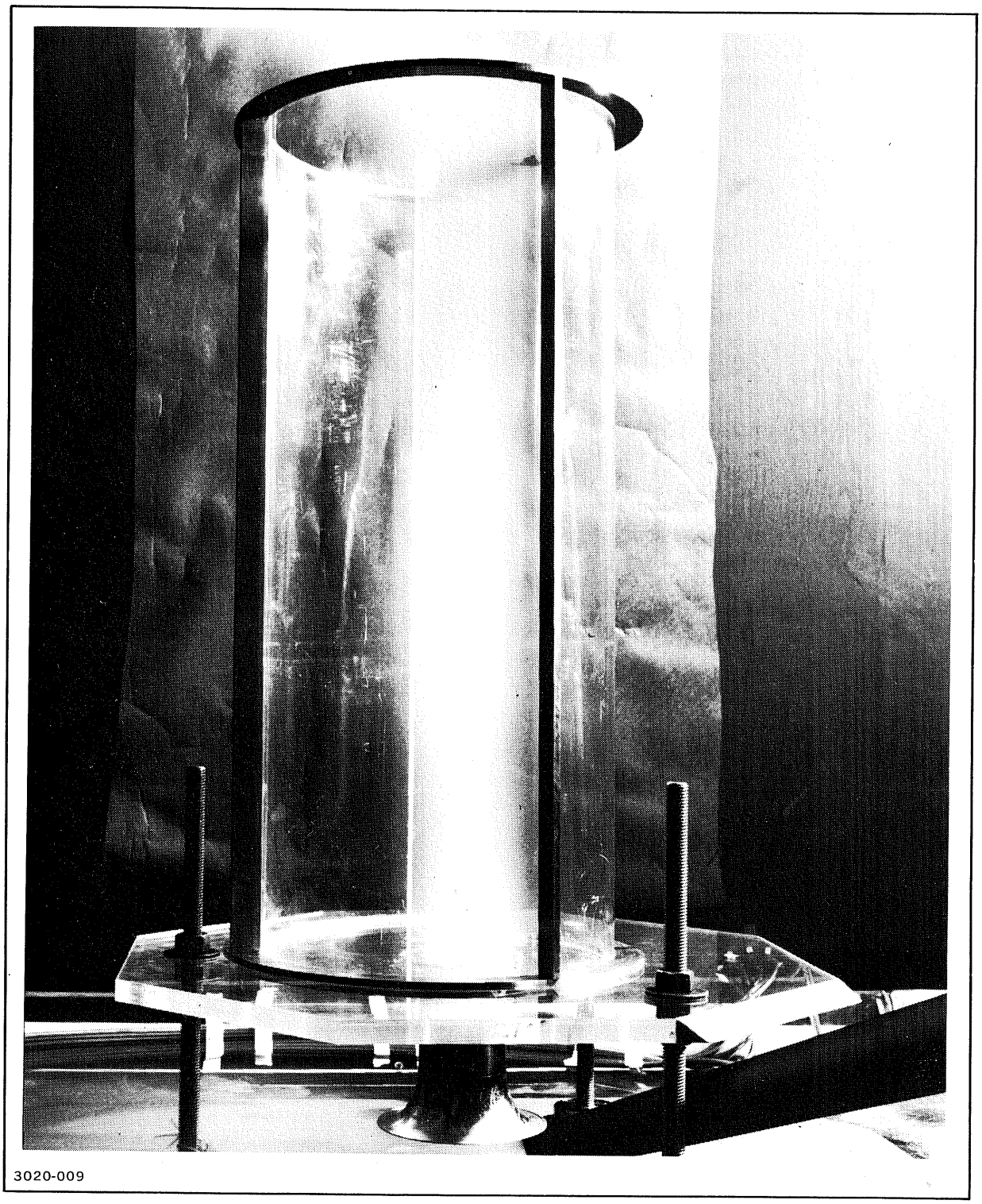

Fig. 9 Flow Visualization of the Vortex Core, with a Screen-simulated Turbine

Fig. 10 Flow Visualization of the Vortex Core, with a Bladed Turbine

is seen to be confined within nearly straight cylindrical columns with sharp boundaries, particularly when a bladed turbine with a stator and a rotor is installed as in Fig. 10. Due to diffusional effects, the vapor column should be larger in size than the vortex core and should enclose the core. Figures 9 and 10 show a clear contraction of the column. Hence, the vortex core also contracts indicating that the vortex is strengthened as it travels upward in the tower. Such a favorable interaction between the tower and the vortex keeps the vortex intact and strong, and prevents "vortex breakdown" within the tower.

We emphasize that the system as a whole interacts with several wind streams and hence can collect wind energy from an area larger than the tower frontal area such that theoretically there is no "Betz Limit" on the power coefficient, C_P, if it is defined based on tower frontal area. As discussed in Ref. 1, the vortex exhausted from the tower interacts strongly with, and gains energy from the wind stream blowing over the top of the tower. The wind stream entering into the side of the tower may have a converging or accelerating streamtube. This enables the system to collect wind energy from an area larger than the tower frontal area. In contrast, the conventional propeller wind turbine collects wind energy from an area smaller than the turbine frontal area and hence has to obey the "Betz Limit".

The analyses of Refs. 6 and 7 (Figs. 11 and 12) show that C_P based on the tower frontal area may exceed the "Betz Limit" of 0.593. The analyses of Refs. 6 and 7 are based on many simplified assumptions but they indicate that theoretically, C_P based on the tower frontal area may achieve a value exceeding not only 0.593 but also unity.

Another point to be covered before the presentation of our experimental results is concerned with the tunnel blockage effect. While this is a complicated effect, Ref. 8 has made a useful analysis for an airscrew or a powered propeller with the results plotted in Fig. 13. For our 25 cm (10 in.) diameter towers, the tower height ranges from 53 to 107 cm (21 to 42 in.) giving an "area fraction" from 6 to 12%. The 13 cm (5 in.) towers have even smaller area fractions. For the largest thrust parameter shown in Fig. 13, it is observed that for an area fraction of 6 to 12%, the blockage effect on the wind tunnel speed V is around 3 to 6%, or around 9 to 19% on both the wind energy density $\frac{1}{2} \rho V^3$ and the power coefficient C_P. The actual blockage effects for

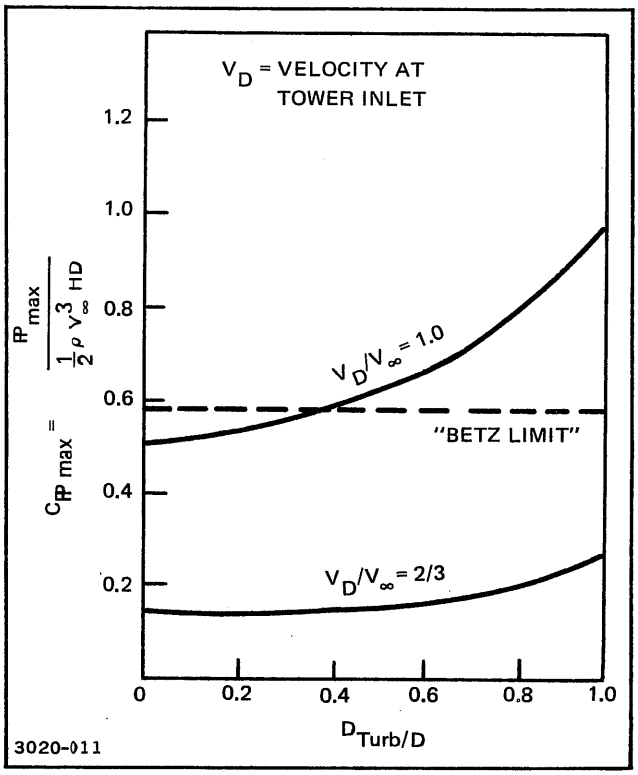

Fig. 11 Theoretical Maximum Power Coefficient Based on Tower Frontal Area (from Ref. 6)

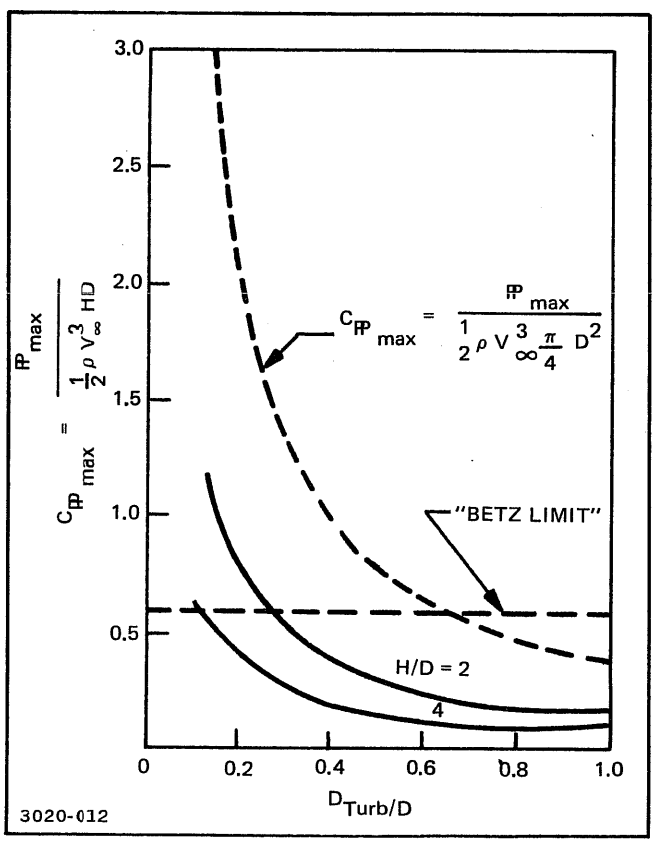

Fig. 12 Theoretical Maximum Power Coefficient Based on Tower Frontal Area (from Ref. 7)

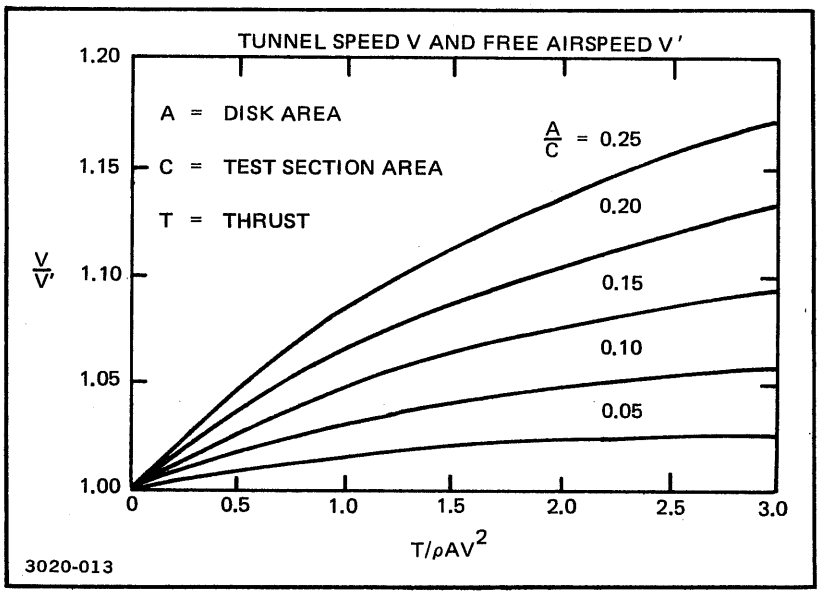

Fig. 13 Tunnel Blockage Effect due to an Airscrew (Ref. 8)

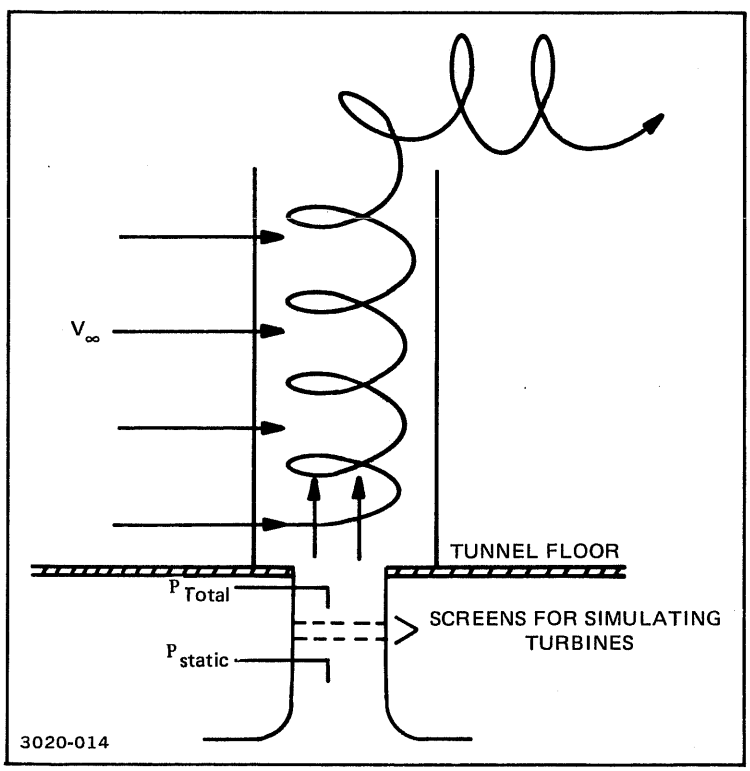

Fig. 14 Experimental Setup with Screen-Simulated Turbine

our towers are expected to be considerably larger than that of an airscrew. But Fig. 13 reinforces our belief that for towers of H = 53 cm (21 in.) and D = 25 cm (10 in.) or smaller, or with area fractions of 6% or less, the blockage effect on the power coefficient C_P would not be excessively large and that the data to be presented on these towers are valid within reasonable uncertainties. The actual blockage effect can be determined only if the same tests are carried out in larger test facilities.

RESULTS

The results presented below were all taken at a wind tunnel speed, V_∞, ranging from 7.8 to 8.1 m/s (17.4 to 18.2 mph). Of course, each data point will be reduced using the appropriate V_∞ recorded for that particular testing.

In order to separate the effects of the bottom inlet geometry, it was decided first to place the tower on the wind tunnel floor, projecting the turbine inlet below the tunnel floor as in previous tests reported in Ref. 1. The setup is sketched in Fig. 14 and some of the models and turbines are shown in Fig. 15. The bottom inlet is then simplified to a single bellmouth followed by a straight section within which the screens for simulating the turbine and the probes for measuring local static and total pressure and local velocity are located. By locating the bottom inlet below the tunnel floor, the clearance above the tower top exit is also increased and the effects due to possible interactions between the exiting vortex and the tunnel ceiling are reduced.

Screens were first used to simulate turbines at different loading coefficients, C_T, defined as

$$C_T \equiv \frac{(\Delta P_t)_{turb}}{\frac{1}{2}\rho V_{turb}^2} \qquad (1)$$

where $(\Delta P_t)_{turb}$ is taken as the difference between the total pressure in the tunnel free stream and the total pressure at the turbine exit, downstream of the screens. This definition was adopted in Ref. 2. It simulates the actual case where a well designed turbine inlet will be located above the ground that maintains a pressure close to the free stream total pressure.

Fig. 15 Towers, Turbines and Generators Used in Tests

The power coefficient is then defined as

$$C_P \equiv \frac{(\Delta P_t)_{turb} \; V_{turb} \; A_{turb}}{\frac{1}{2} \rho V_\infty^3 H D} \qquad (2)$$

where V_{turb} is the flow velocity through the turbine. The power developed by the vortex and imparted to the turbine is equal to the product of the difference in total pressure across the turbine and the flow rate through the turbine. The power output of the system is equal to the above power times the mechanical efficiency of the turbine and the electrical efficiency of the generator. The turbine, being enclosed within the bottom inlet can have a much better mechanical efficiency than an open turbine since the tip losses, which are associated with the shedding of vortices from the tips of the turbine blades and which are the principal losses of an open turbine, have been eliminated. It has been shown in Ref. 9 that such a turbine can achieve a mechanical efficiency of better than 90%. A standard electrical generator can have a similar efficiency in converting mechanical into electrical energy. Hence, thepower output of our system can be close to the power made available by the vortex. The power coefficient of the system may be represented, within experimental accuracy, by Eq. (2).

The results on C_P are presented in Figs. 16 to 23 and summarized in Figs. 24 and 25. The data are taken with two groups of towers, one with a 12.7 cm (5 in.) diameter and 25.4 to 53.3 cm (10 to 21 in.) in height, and the other with a 25.4 cm (10 in.) diameter and 53.3 cm to 106.6 cm (21 to 42 in.) in height. Both groups have a spiral cross section as shown in Fig. 4 which also defines the diameter. Figures 16 to 18 and 21 to 22 show the effects of changes in turbine sizes on C_P, in the same tower. The data points represent values of C_P plotted versus the turbine disk loading C_T, with the turbine size as a parameter. C_T is varied by changing the mesh size and the number of the screens which simulate a turbine. For each of these figures, the peak value of C_P based on the turbine area is also given on each curve. These figures show that generally, C_P based on the turbine area attains a higher value for a smaller turbine for the same tower. On the other hand, C_P based on the tower frontal area HD is higher for a larger turbine, again for the same tower.

A smaller turbine would be more completely concentrated in the strongest part of the low pressure vortex core, resulting in a higher pressure difference across the turbine and a better performance. However, the ratio of the turbine

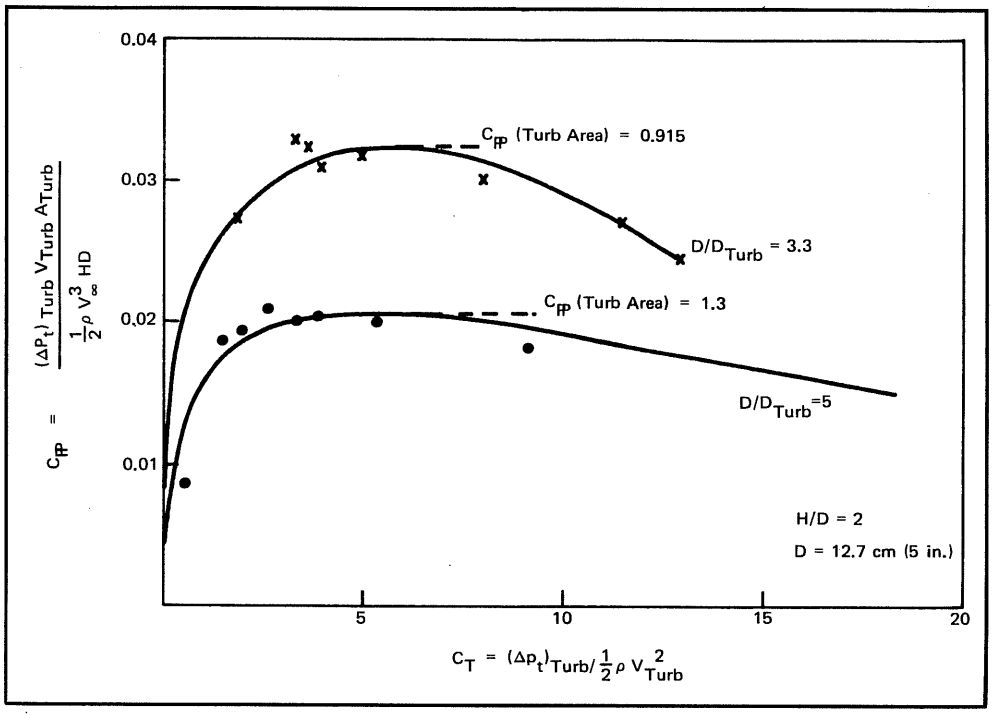

Fig. 16 Plot of Power Coefficient C_{FP} versus Disk Loading Coefficient C_T for D = 12.7 cm (5 in.), H/D = 2 and Different D/D_{Turb} Ratios.

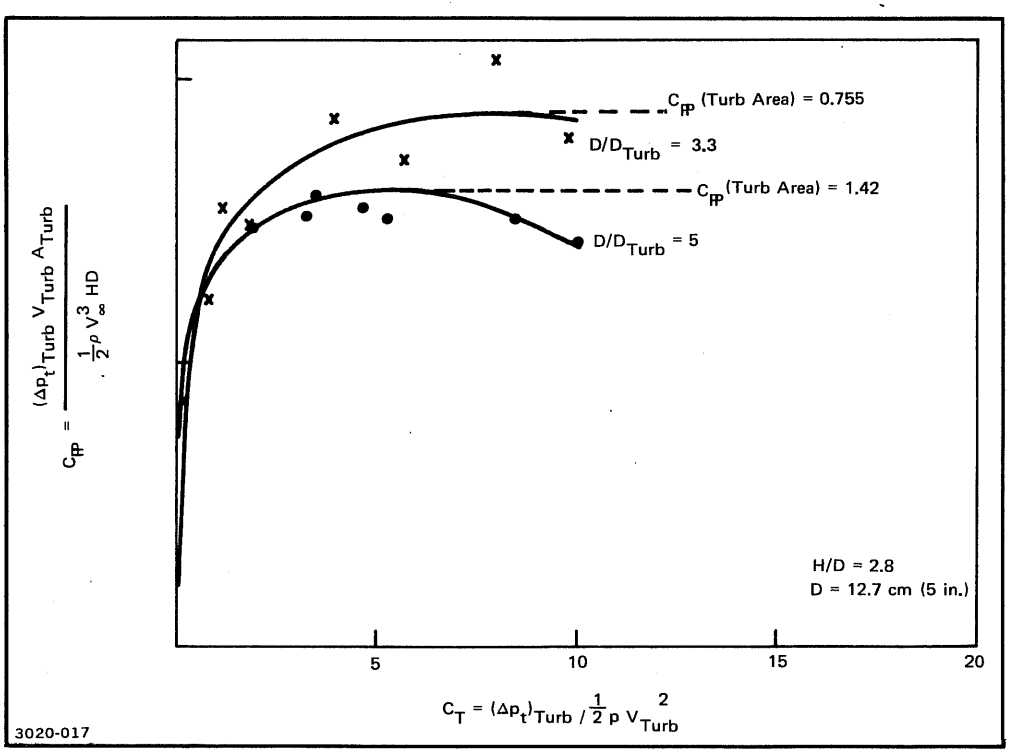

Fig. 17 Plot of Power Coefficient C_{FP} versus Disk Loading Coefficient C_T for D = 12.7 cm (5 in.), H/D = 2.8 and Different D/D_{Turb} Ratios.

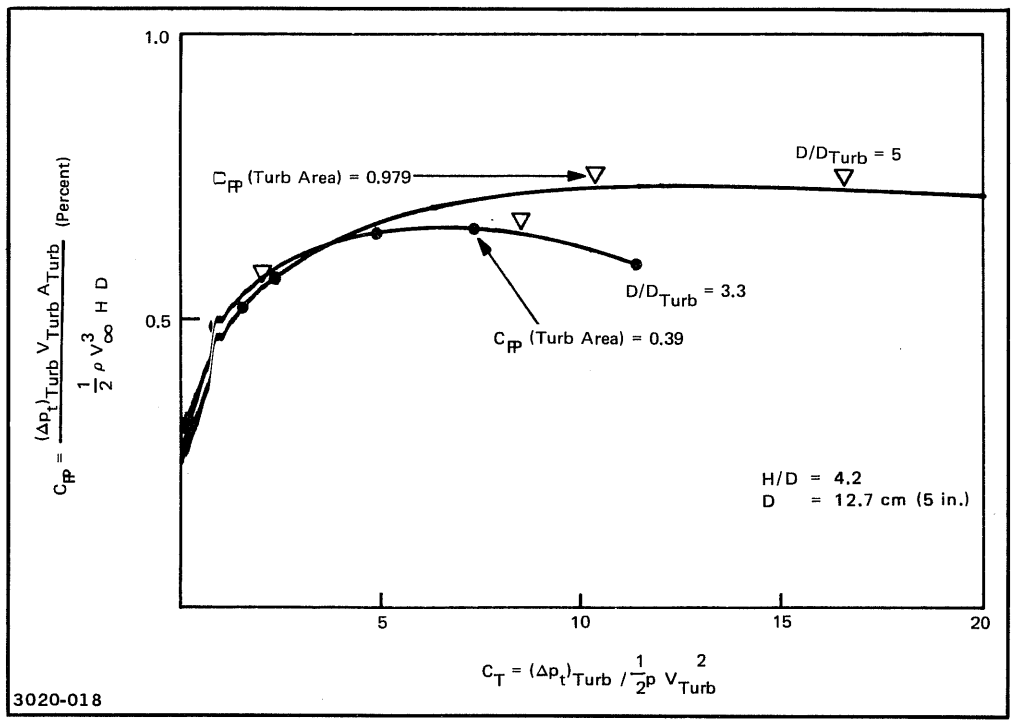

Fig. 18 Plot of Power Coefficient C_{FP} versus Disk Loading Coefficient C_T for D = 12.7 cm (5 in.), H/D = 4.2 and Different D/D_{Turb} Ratios.

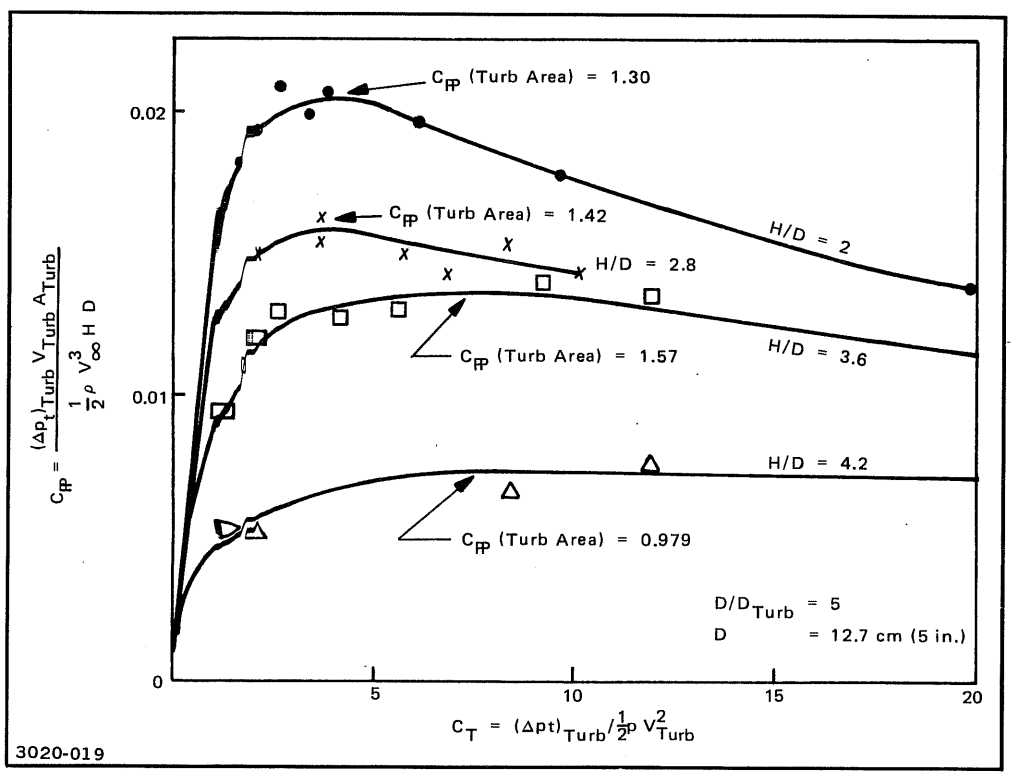

Fig. 19 Plot of Power Coefficient C_{FP} versus Disk Loading Coefficient C_T for D = 12.7 cm (5 in.), D/D_{Turb} = 5 and Different H/D Ratios

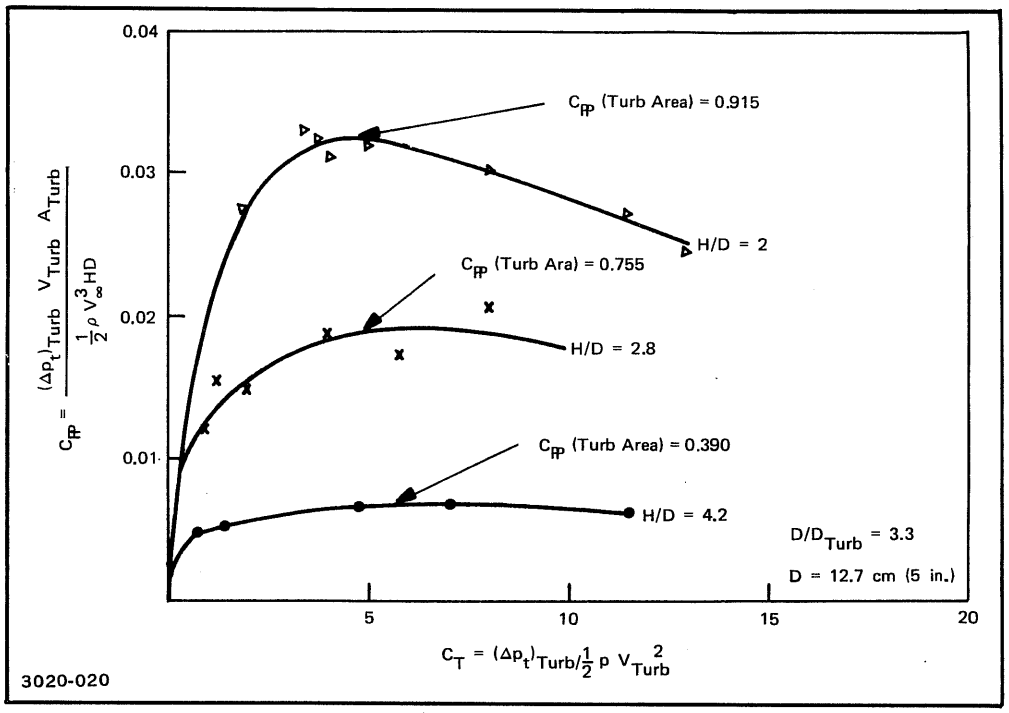

Fig. 20 Plot of Power Coefficient C_{FP} versus Disk Loading Coefficient C_T for D = 12.7 cm (5 in.), D/D_{Turb} = 3.3 and Different H/D Ratios

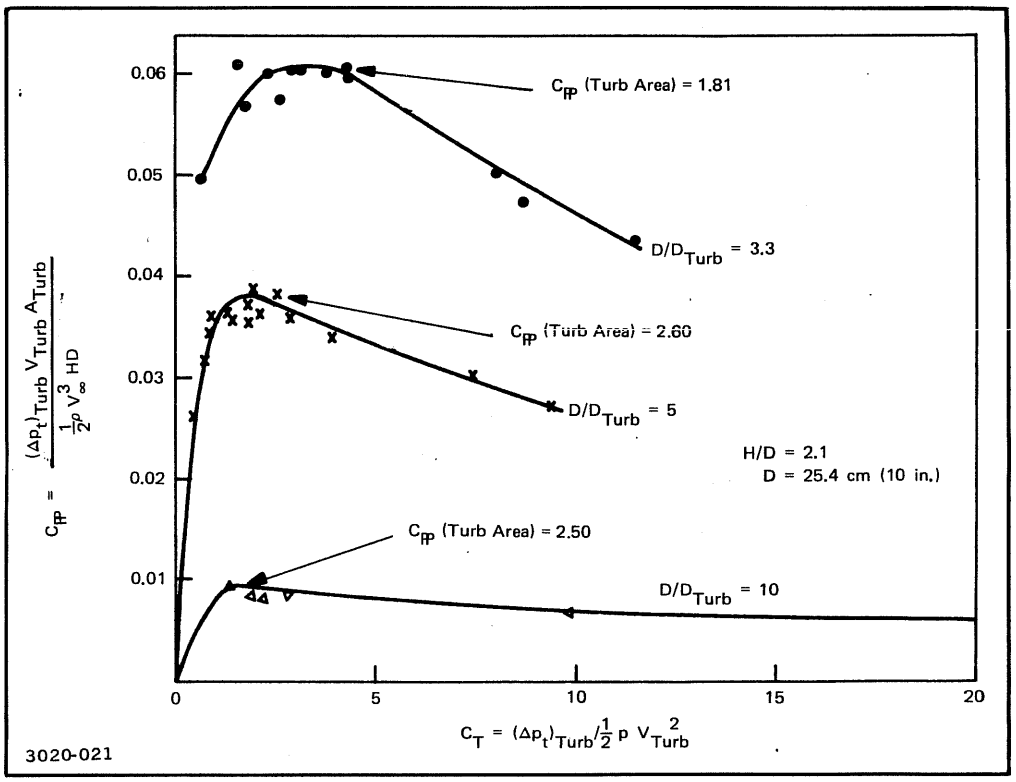

Fig. 21 Plot of Power Coefficient C_{FP} versus Disk Loading Coefficient C_T for D = 25.4 cm (10 in.), H/D = 2.1 and Different D/D_{Turb} Ratios

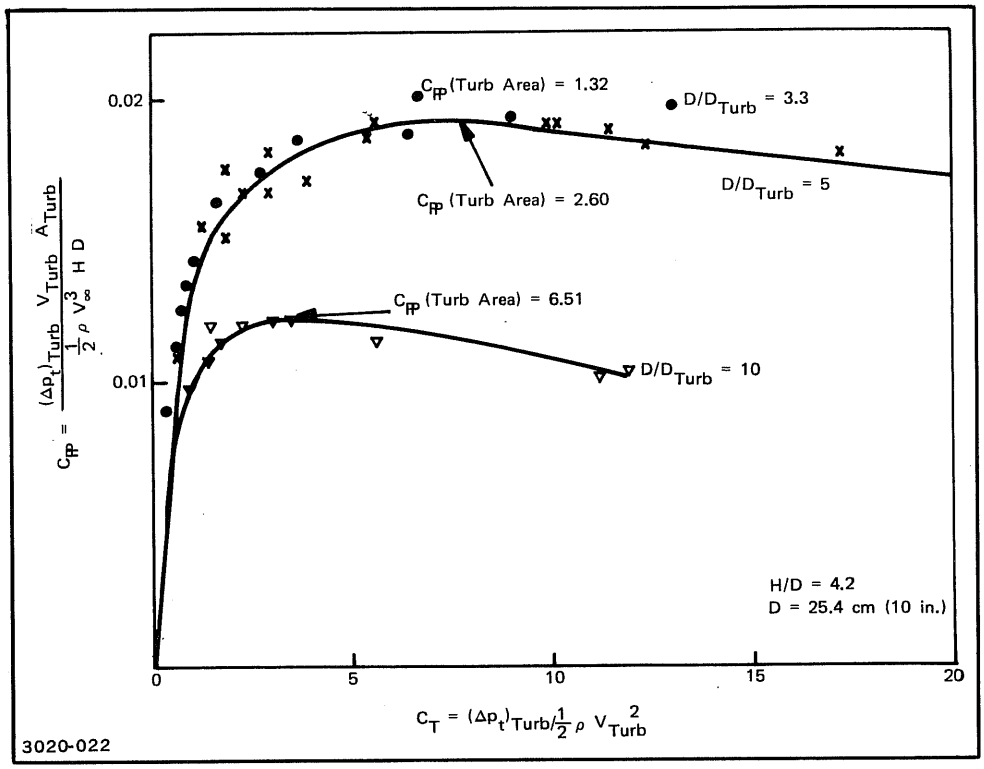

Fig. 22 Plot of Power Coefficient C_{FP} versus Disk Loading Coefficient C_T for D = 25.4 cm (10 in.), H/D = 4.2 and Different D/D_{Turb} Ratios

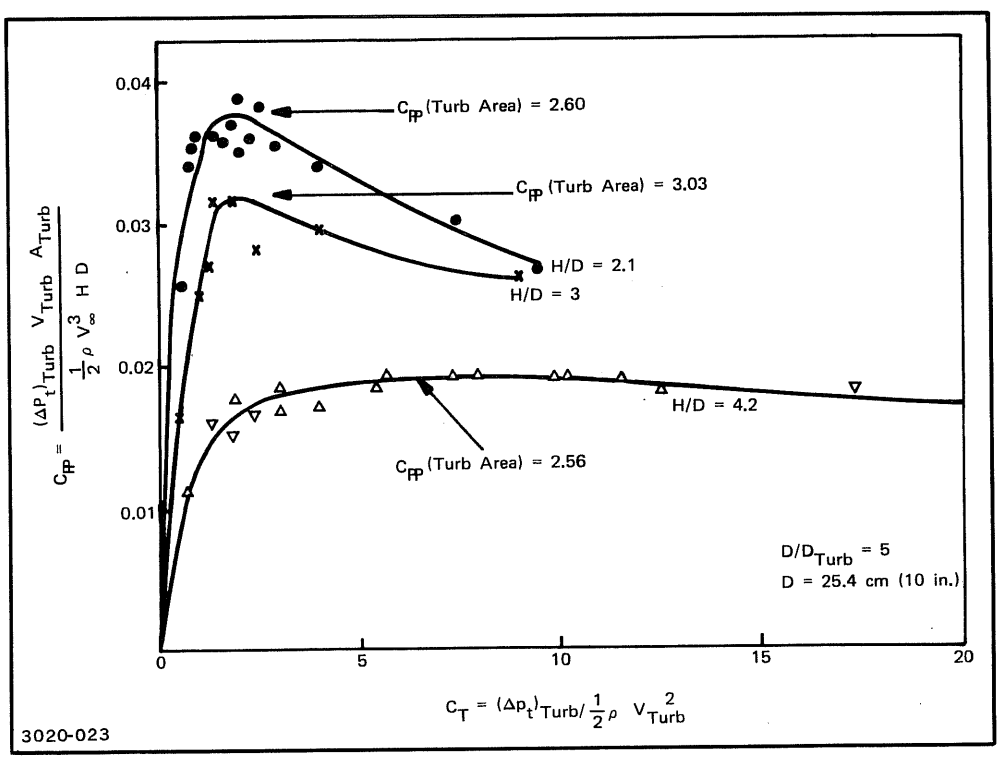

Fig. 23 Plot of Power Coefficient C_{FP} versus Disk Loading Coefficient C_T for D = 25.4 cm (10 in.) D/D_{Turb} = 5 and Different H/D Ratios

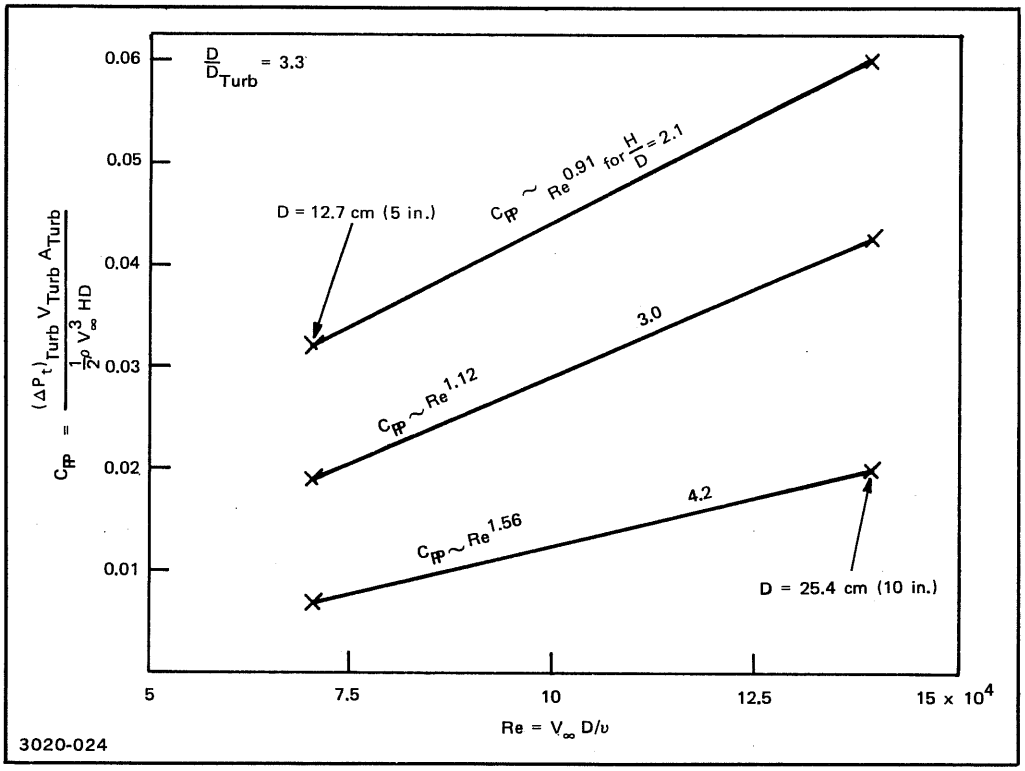

Fig. 24 Scaling Law, Plot of Power Coefficient C_{FP} versus Reynolds Number Re for D/D_{Turb} = 3.3 and Different H/D Ratios

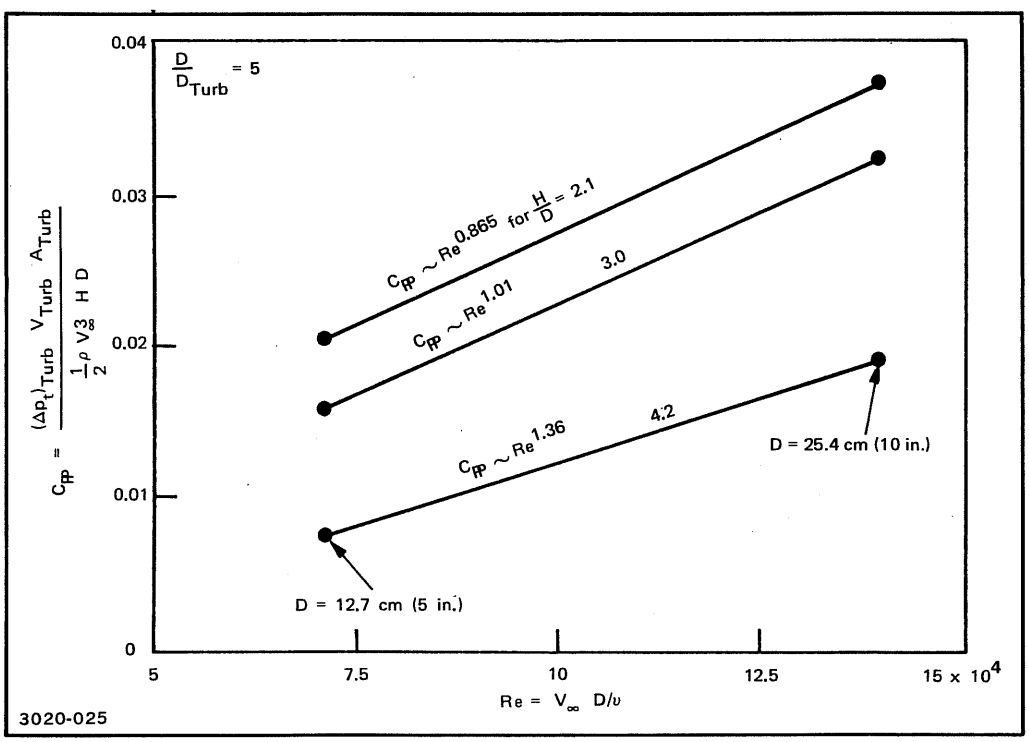

Fig. 25 Scaling Law, Plot of Power Coefficient C_{FP} versus Reynolds Number Re for D/D_{Turb} = 5 and Different H/D Ratios

area to the tower frontal area decreases the power coefficient as the square of its radius, when compared with a larger turbine. Hence, the power coefficient degrades with diminishing turbine size when it is computed on the basis of the tower frontal area.

The best C_P based on the turbine area is given by Fig. 22 with a value of 6.51 for a tower of $H/D = 4.2$, $D/D_{Turb} = 10$ and $D_{Turb} = 2.5$ cm (1 in.). This gives an augmentation ratio of around 20 when compared with a conventional horizontal-axis wind turbine which usually has a C_P of around 0.30 based on the turbine disk area. When compared on the basis of the tower frontal area, the shortest tower of Fig. 11 gives the highest value of around 6% for C_P, with $H/D = 2.1$, $D/D_{Turb} = 3.1$ and $D_{Turb} = 7.6$ cm (3 in.). This value is already larger than the 0.033 "maximum" performance limit which Loth (Ref. 6) has predicted. (Results of Loth's analysis have been reproduced as Fig. 11 which shows a range of 0.15 to 1.00 for C_P according to his analysis. He then assumed that performance will be severely affected by various energy loss mechanisms and came up with a performance limit of $C_P = 0.033$ for practical machines.)

The data are replotted in Figs. 17, 18 and 21, based on the same turbine size and the same D/D_{Turb}, but for different tower heights. It is seen that generally, a shorter tower gives a better C_P based on the tower frontal area but the converse is true for C_P is based on the turbine area.

For C_P based on the tower frontal area, the data are replotted to show the "scaling law" in Figs. 24 and 25 for D/D_{Turb} of 3.3 and 5, respectively. The peak value of C_P on each of the curves of the previous figures are used in plotting Figs. 24 and 25. They show clearly that a shorter tower with a larger turbine gives a better C_P based on the tower frontal area. Moreover, C_P improves strongly when the tower size or the Reynolds number (Re) is increased keeping the same geometry or the same H/D and D/D_{Turb}.

It is seen that C_P varies as Re to the power between 0.86 and 1.56. From an engineering "rule of thumb", it is generally expected that C_P would vary as Re to the power of around 0.2 to 0.3. Hence, our data have shown a very strong scaling law. Even the lowest powers of 0.86 and 0.91, given by short towers of 25 to 53cm (10 to 21 in.) in height, are much larger than 0.2 or 0.3.

Since the full scale systems would be of tens to hundreds times larger than our models, we can expect that C_p of the full scale system will be much larger than the values we reported. Systems of around 100 MW in generating capacity may be achievable with a reasonable tower size, as will be discussed later.

We next point out a discrepancy between the above results and our previous data (Ref. 3) taken in a smaller 0.6 to 0.9 m (2 x 3 Ft) wind tunel at a 5.8 m/s (12.8 mph) wind speed. As illustrated in Fig. 26, there is a discrepancy in power coefficient around three times for the same model when tested in the two different tunnels. We have investigated various possible causes of this large discrepancy and have found that by enclosing the entire system within the 1.2 x 1.8 m (4 x 6 Ft) wind tunnel, a large fraction of this discrepancy may be removed. A report on the findings will be issued at the completion of these investigations.

Another set of experiments is carried out with crude turbines to replace the screens. Thrust and rpm developed by the turbines are measured together with the flow velocity through the turbine. A DC electrical generator with resistive loads was connected to the turbine as shown in Fig. 27. The generator is precalibrated to give a measured generating efficiency as a function of RPM and load resistance.

The product of the thrust and the flow velocity through the turbine gives the mechanical power input into the turbine from the vortex. Electrical power output from the generator is given by E^2/R when E is the voltage generated across the load resistance R. The ratio between the electrical power output and the mechanical power input is equal to the product of the mechanical efficiency of the turbine and the electrical generating efficiency of the generator. Since the latter has been measured, we can compute the mechanical efficiency of the turbine.

For our enclosed turbine, it has been mentioned previously that the turbine has no significant tip loss and can have a high mechanical efficiency (Ref. 9). Our actual turbines, however, are limited to 5 to 10 cm (2 to 4 in.) in diameter. They suffer greatly in aerodynamic performance, tip-speed-ratio, and in mechanical efficiency because they operate at very low Reynolds numbers.

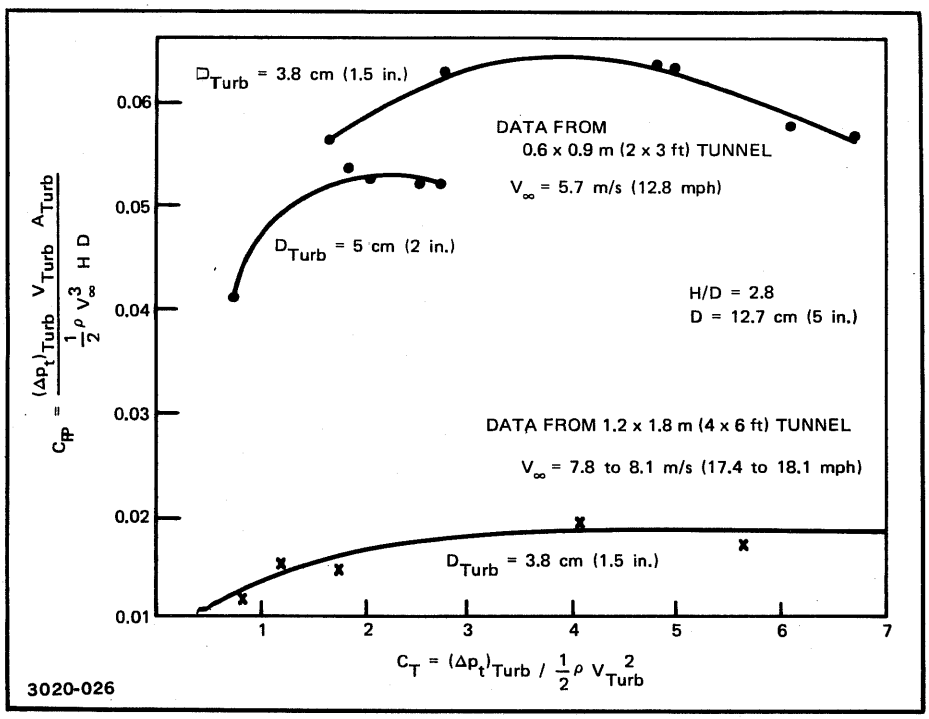

Fig. 26 Comparison of Data From 1.2 x 1.8m (4 x 6 ft) tunnel with Previous Data from .6 x .7m (2 x 3 ft) tunnel with the same Model

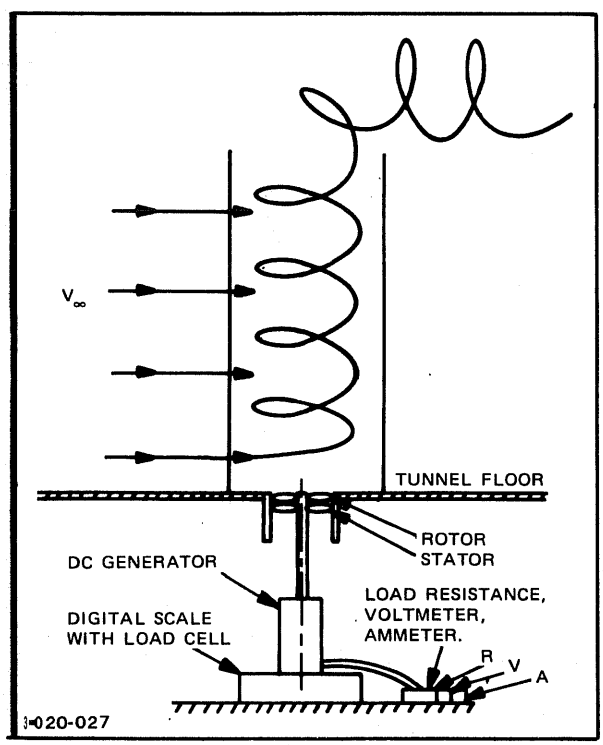

Fig. 27 Experimental Setup with Bladed Turbine and Electrical Generator

To avoid unnecessary mechanical complications, the rpm has been restricted to 5000 or less, with 2000 to 4000 as the range of rpm under load. This, and the small sizes of the turbines, combine to yield very low chord Reynolds numbers of 4 to 8 x 10^3 for the 5 cm (2 in.) turbines and 2 to 4 x 10^4 for the 10 cm (4 in.) turbines. They also limit the tip-speed-ratio (defined in Eq. (3)) to low values between 1 and 2, instead of the usual 4 to 5 or higher required for an efficient turbine.

The very low chord Reynolds numbers prevent us from utilizing the standard aerodynamic performance data (lift and drag coefficients versus the angle of attack) of standard airfoils which are valid only for chord Reynolds numbers of 10^6 or higher. We therefore cannot carry out a detailed design to determine the suitable airfoil cross section for the turbine blades. It is well known that at very low chord Reynolds numbers such as ours, the lift coefficient of any airfoil is much lower, the drag coefficient much higher, and the stall angle much smaller, than the standard cases at high chord Reynolds numbers. Moveover, the pressure fields in the vortex and around the turbine blades are interacting. Hence, poor aerodynamic performance of the blades may degrade the power input from the vortex as will be seen from Figs. 29 and 31 discussed below. In other words, a larger system with a well designed turbine should have a better power performance than our crude system due to improved turbine performance. Hence, aside from the strong scaling laws as reported in Figs. 24 and 25, this gives an additional indication that the system performance should improve with the size of the system. Our turbine, which has a stator and a rotor combination, is designed only in terms of overall inlet and outlet flow angles. The turbines are made by using available sheet metal fan blades and by twisting the blades backwards to obtain the design flow angles.

We compute our power coefficient based on the power input from the vortex, since for larger systems the turbine as well as the generator can have high efficiencies as we have discussed above. The data are shown in Figs. 28 to 33. For the 10 cm (4 in.) turbine, we tested only the one designed with $C_T = 3$ and $X = 1$ where C_T is the turbine disk loading coefficient defined in Eq. (1) and X is the tip-speed-ratio defined as

$$X = \pi n \, D_{Turb}/V_{Turb} \tag{3}$$

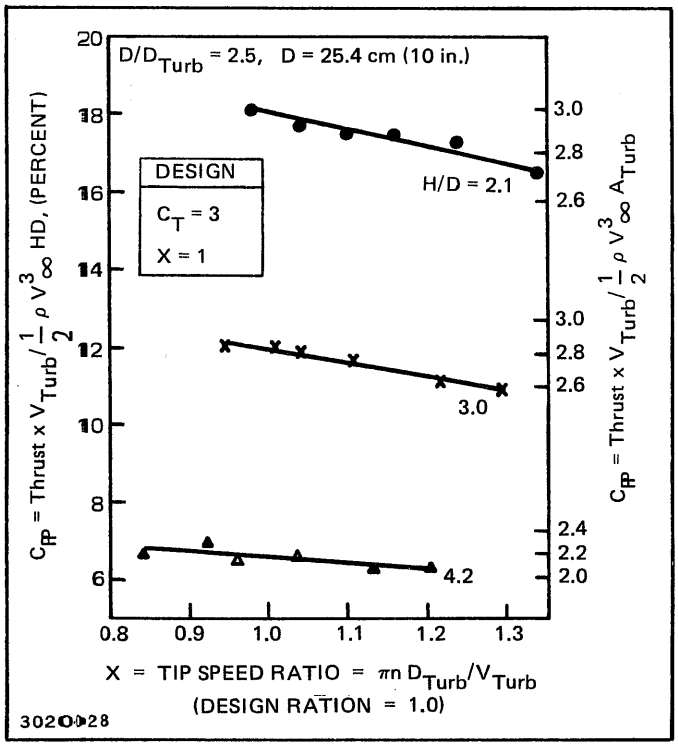

Fig. 28 Plot of Power Coefficient C_P versus Tip Speed Ratio X for D = 25.4 cm (10 in.), D/D_{Turb} = 2.5 and Different H/D Ratios

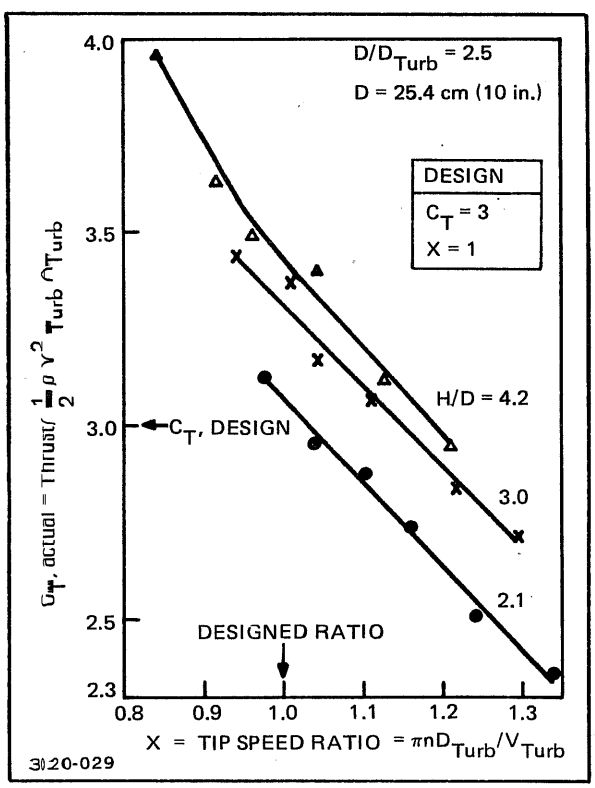

Fig. 29 Plot of Measured Disk Loading Coefficient versus Tip Speed Ratio for the Cases of Fig. 28

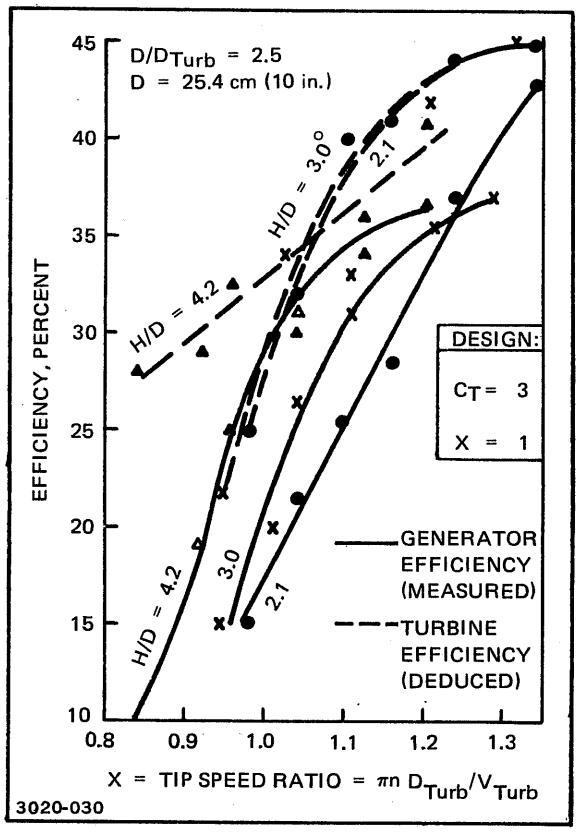

Fig. 30 Plot of Generator and Turbine Efficiencies versus Tip Speed Ratio for the Cases of Fig. 28

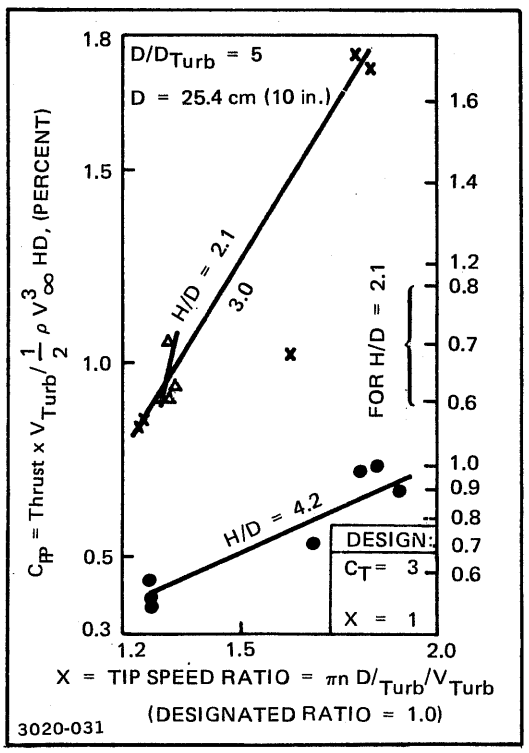

Fig. 31 Plot of Power Coefficient C_{PP} versus Tip Speed Ratio X for D = 25.4 cm (10 in.), D/D_{Turb} = 5 and Different H/D Ratios

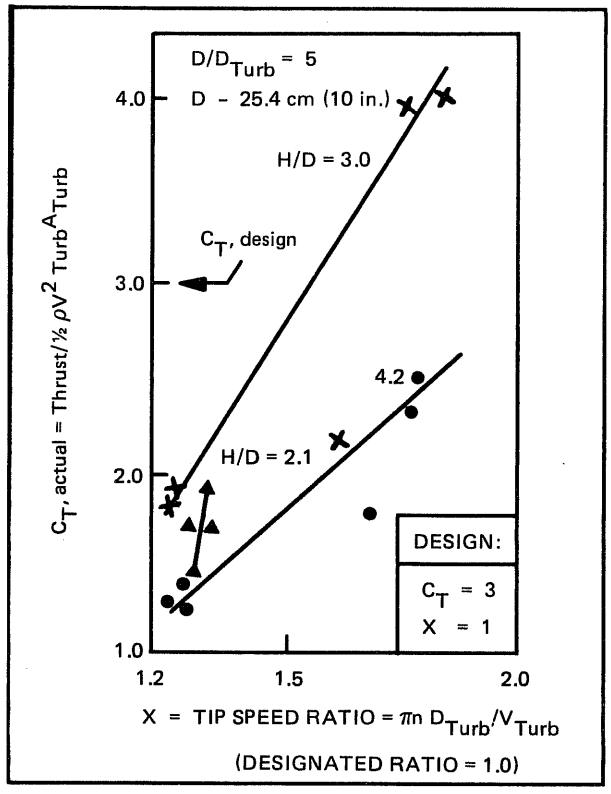

Fig. 32 Plot of Measured Disk Loading Coefficient versus Tip Speed Ratio for the Cases of Fig. 31

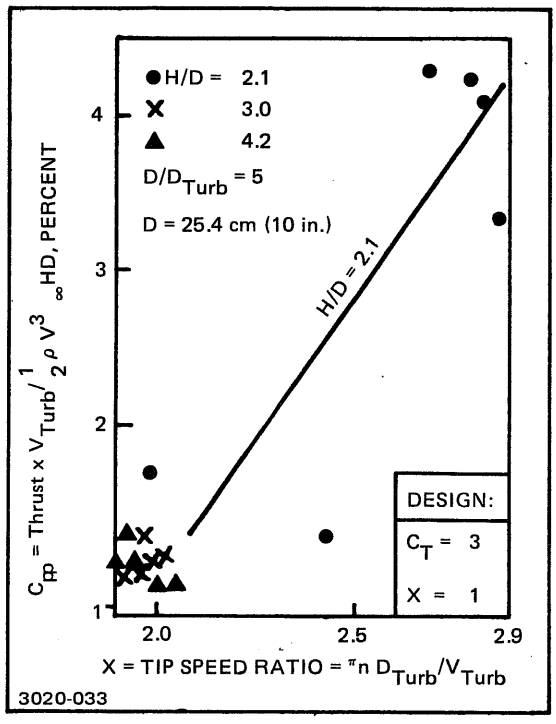

Fig. 33 Plot of Power Coefficient C_{pp} versus Tip Speed Ratio X for C_T = 10 and X = 2, D/D_{Turb} = 5 and Different H/D Ratios

with n denoting the rpm of the turbine. For the 5 cm (2 in.) turbine, we tested with $C_T = 3$ and $X = 1$ and with $C_T = 10$ and $X = 2$. We will carry out additional testings in the next contract.

Figures 28, 31, and 33 show the power coefficient C_P for the three turbines tested. The best C_P of 18% comes from the short tower of Fig. 28 with $H/D = 2.1$, $D/D_{Turb} = 2.5$ and $D_{Turb} = 10$ cm (4 in.). This value is better than those given by the screen-simulated turbines of Figs. 16 through 26. It reflects a favorable interaction between the vortex and turbine. The turbine which rotates in the opposite sense to the vortex, imparts an angular momentum into its exhaust flow in the same direction as the vortex. In contrast, the exhaust from a screen-simulated turbine has no angular momentum and therefore tends to slow down the vortex when it merges with and attains the same rotating speed as the vortex. This favorable effect is also visualized in Figs. 9 and 10, where it is seen that with a bladed turbine, the smoke column is much more dense or concentrated.

Comparison of Figs. 31 and 33 shows that the turbine design affects the power input from the vortex. Figure 33, with a 5 cm (2 in.) turbine designed $C_T = 10$ and $X = 2$, shows a better performance than Fig. 31, with another 5 cm (2 in.) turbine designed at $C_T = 3$ and $X = 1$. It is believed that the higher tip-speed-ratio X is mostly responsible for the improvement. The data on the 5 cm (2 in.) turbines are quite erratic and less useful. One reason is that at the lower levels of thrust from the smaller turbines, the data are more affected by the fluctuations in the thrust.

With such crudely designed turbines, it is quite surprising that the measured C_T and X as displayed on Figs. 29, 32, and 34 come quite close to their design values. Figures 32 and 34 are for the same sized turbines. The measured values of C_T and X, however, are greatly different for the two figures. It is believed that it is not accidental that the actual values follow closely the designed values, since all three cases display the same behavior. It is believed that this means that the turbine design is not "fussy" or troublesome. It is hoped that these trends will sustain in the future to alleviate the difficulties in system development.

While the data from the 5 cm (2 in.) turbines are erratic, those from the 10 cm (4 in.) turbines are quite systematic. The efficiencies of the turbine

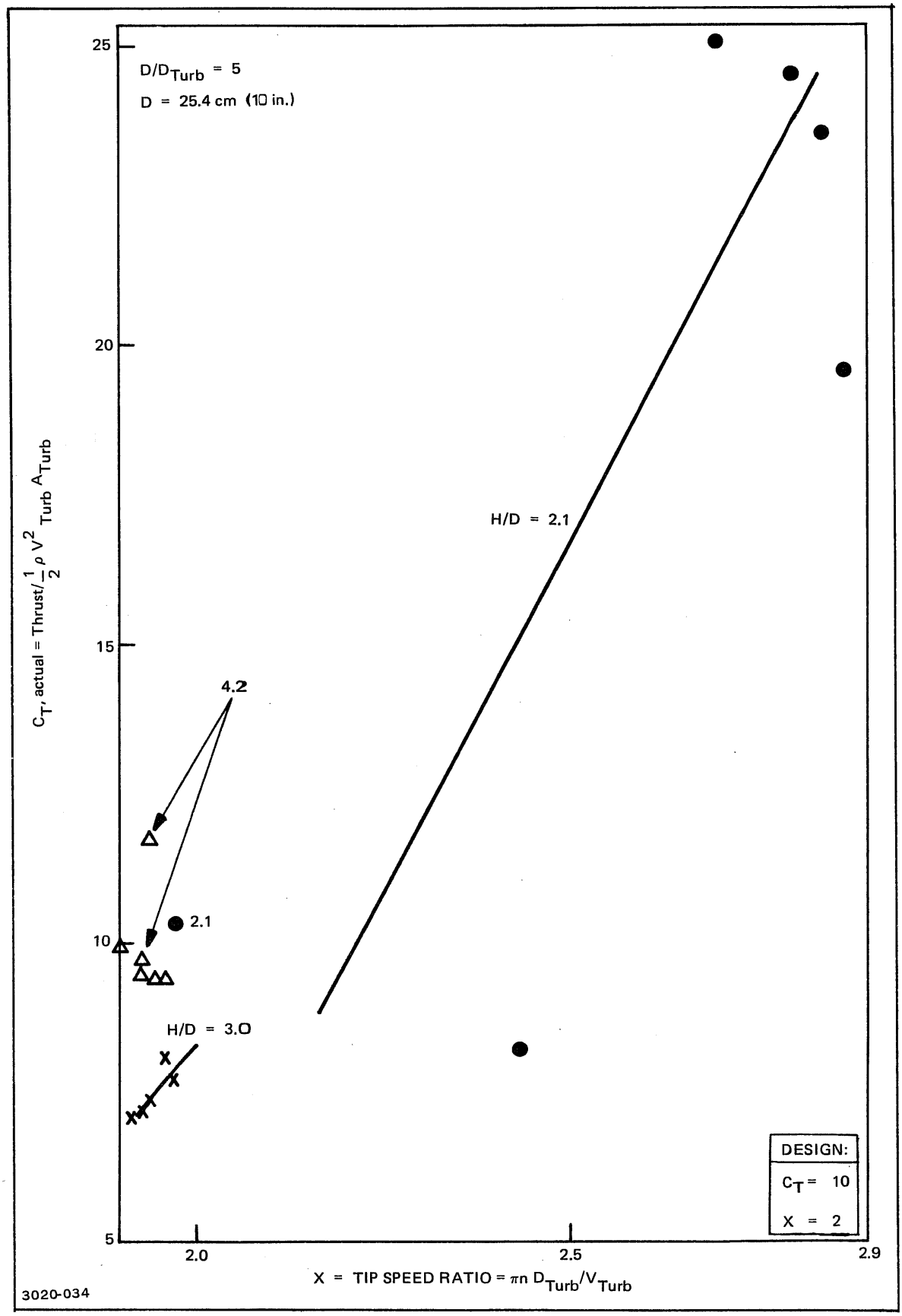

Fig. 34 Plot of Measured Disk Loading Coefficient versus Tip Speed Ratio for the Cases of Fig. 33

and the generator are plotted versus the tip-speed-ratio on Fig. 30. The generator efficiency is measured by a calibration while the turbine efficiency is deduced as we have mentioned previously. It is seen that both efficiencies improve with the tip-speed-ratio and that even with crudely designed turbines, a turbine efficiency of around 45% has been achieved.

Summarizing, we have obtained a best value of 6.51 for C_P based on the turbine area, an augmentation ratio of around 20, and a best value of around 18% for C_P based on the tower frontal area. Also, we have obtained strong scaling laws with C_P increasing as Reynolds number to the power of 0.86 to 1.56. These scaling laws are derived from testing tower models of 13 and 25 cm (5 and 10 in.) in diameter, while the working full scale system would be of tens to hundreds meters in diameter, or a tens- or hundreds-fold increase in size and Reynolds number from the tested models.

SCALING TO LARGER SIZES

Although scaling trends of the small-scale tests available to date are extermely encouraging, any extrapolation of those trends over large size ranges is necessarily speculative. Nevertheless, we feel it is essential to try to give some measure of the potential of the concept in large sizes, even though there will be no way of being accurate until data are available at significantly larger Reynolds numbers.

There are two basic scaling trends to be exploited. The first is the increase in wind available due to increased height of the tower, which depends on the atmospheric wind profile and the degree to which vortex strength aloft is coupled to the turbine. This will be discussed first, using the assumption that the turbine will respond to the integrated power over the tower frontal area. We have only qualitative demonstrations to support this particular scaling, but it is not unreasonable in the light of our current knowledge of the vortex mechanics in the device.

The second scaling trend is the proven improvement in vortex strength with increasing Reynolds number. This is the most important technical issue in the entire project, and is discussed in several other places in this report. The measured trends discussed above are so strong that they could not responsibly be used for scaling to large units without a great deal more support. They are

characteristic of the trends one would find in a laminar region, where vortex strength increases directly with size. In fully turbulent regions, the size growth trend will be much weaker, perhaps disappearing altogether. Furthermore, late in our testing program for the first phase we discovered that our tower vortex was greatly influenced by the wind tunnel floor boundary layer, which occupies a greater portion of the frontal area of the smaller (lower Re) towers. We revised our model mount, and found that, at least in the one case tested so far, the Reynolds number trend was essentially undiminished. Finally, there is always the possibility that performance improvement with Re will continue only up to a level of power coefficient at which some other, nonviscous, mechanism will limit performance. Given all of these concerns, we can still safely assert that large scale systems will perform significantly better than current small scale models.

For the purposes of estimating the growth potential of the TWES, we have used the scaling law of $C_{\mathbb{P}} \sim Re^m$ with m = 0.2 to 0.3, down from the small scale results where m = 0.86 to 1.56. Hence, as a conservative estimation, we have used an "average" scaling law with m = 0.2 to 0.33 spanning the entire range from the small models, to full-size systems (e.g., D = 150 m (500 Ft)). The results are presented below.

The calculation for the power output for a large system should include a factor F(H) which accounts for the increase in wind speed with height, or

$$\mathbb{P} = (\tfrac{1}{2}\,\rho\, V_R^3) \cdot F(H) \cdot HD \cdot C_{\mathbb{P}} \tag{4}$$

where

$$F(H) = \frac{H_o}{H} \int_1^{1+H/H_o} (V/V_R)^3 \, d(Z/H_o) \tag{5}$$

V_R is the rated wind speed at the usual height of H_o = 9 m (30 Ft) and H is the tower height. The function represents then the average wind energy intensity over the tower. For the conventional wind turbine, different formulations for F(H) are used in the power ratings listed in Refs. 10 and 11.

Before we evaluate F(H), we mention that diurnal variations in wind profiles are discussed in Ref. 12. During the evening, through the night and morning, turbulent mixing due to solar heating stops and winds at altitudes of 10 to 500 m (30 to 1500 Ft) are released from the constraints of surface friction.

Such "decoupled" winds are then free to accelerate in response to existing pressure gradients, and a nocturnal wind maxima is produced as shown in Fig. 35. The wind speed increases with height at a pace much faster than the usual one-seventh power law and may achieve a one-half power law. During daytime, solar heating induces a "coupling" or a constant exchange of momentum between the upper and the near-surface winds through turbulent mixing. The upper winds are then constrained by surface friction and the nocturnal wind maxima dissappears. Over open terrain, wind profiles measured in daytime under well-mixed conditions are found to correspond to the one-seventh power law, as shown in Fig. 36, and discussed in Refs. 12 and 13.

Taking a more conservative case of one-seventh power law, Eqs. (4) and (5) are evaluated with results given in Table 1.

TABLE 1 ESTIMATED POWER OUTPUT FOR A FULL-SCALE SYSTEM
(Based on an Average Scaling Law of $C_P \sim R_e^m$)

Exponent, m	C_P	Estimated Power Output
0.2	0.69	90 MW
0.25	0.89	110
0.3	1.23	150
0.33	1.50	190
for H = 300 m (1000 Ft), D = 150 m (500 Ft), D_{Turb} = 60 m (200 Ft) and a spiral cross section with V_R = 11 m/s (25 mph) at 9 m (30 Ft) altitude.		

The basis for Table 1 is the "average" scaling law $C_P \sim R_e^m$ together with the value of $C_P = 0.18$ which is given by Fig. 27 for the small model (H/D = 2.1, $D/D_{Turb} = 2.5$ and $D_{Turb} = 2.5$ and $D_{Turb} = 10$ cm (4 in.) or H = 53 cm (21 in.) and D = 25 cm (10 in.).

We mention that $\frac{1}{2} \rho V_\infty^3 = 0.83$ kW/m^2 (0.077 kW/ft^2) for V_R = 11 m/s (25 mph) and F(H) = 3.26 for H = 300 m (1000 Ft). In comparison, for the Mod-1 propeller turbine, in order to generate the rated 2 MWe with 60 m (200 Ft) diameter blades and with the same rated wind speed of V_R = 11 m/s at 9 m (25 mph at 30 Ft) as listed in Ref. 11, one needs a F(H) value of 2.77 for $C_P = 0.2$, and F = 2.06 for $C_P = 0.4$. Note that usually C_P is less than 0.4 for such turbines, and that the tip of the Mod-1 blades reaches only up to an altitude of H = 73 m (240 Ft). Referring to Table 1, it is seen that for our "average" scaling

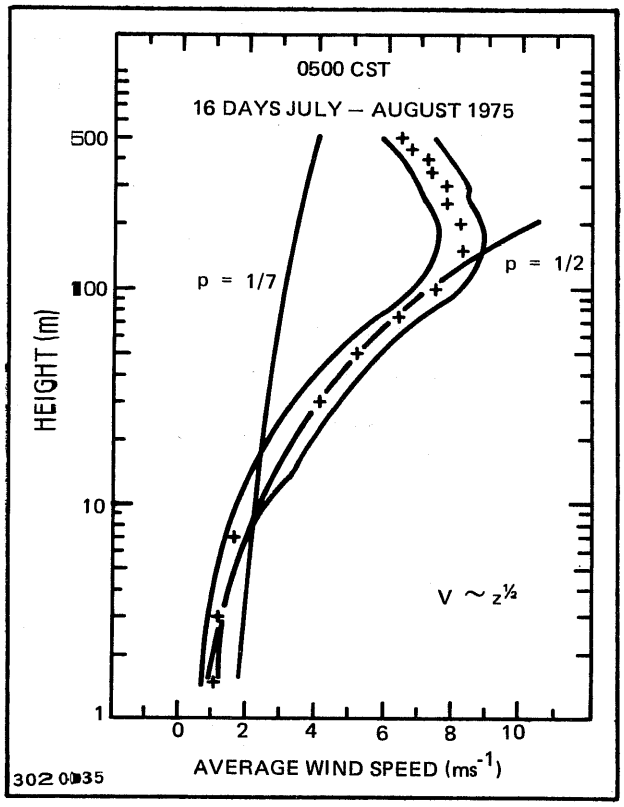

Fig. 35 Variation of Wind Speed with Height, Exhibiting the Nocturnal Boundary-layer Maxima

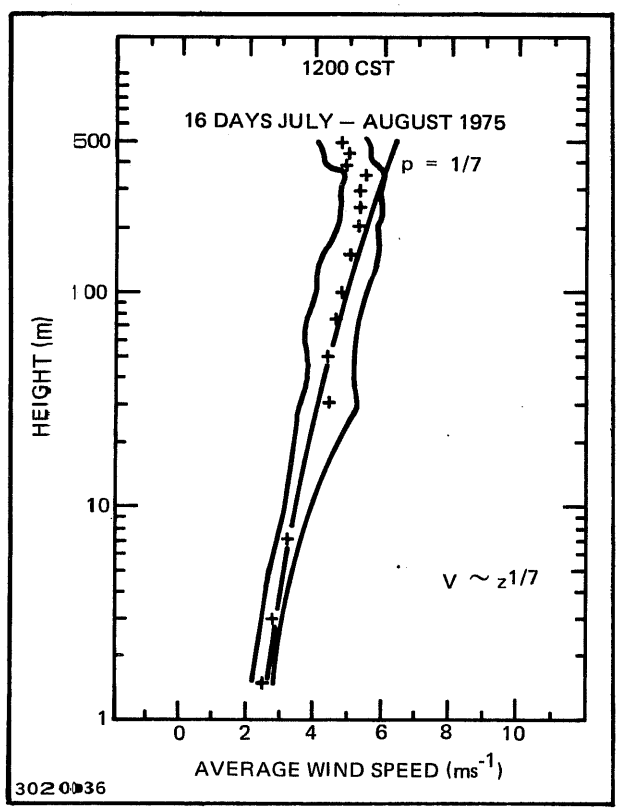

Fig. 36 Variation of Wind Speed with Height, Exhibiting the Noon Time Boundary-layer Maxima

law with m = 0.2 to 0.33, the power output may reach 100 to 200 MW with a reasonably sized tower.

We should point out that the models tested all have a spiral cross section with a fixed side inlet covering around 25% of the tower frontal area. The original design however, calls for a multiple vaned tower capable of achieving an inlet area equal to or exceeding the tower frontal area. Such a tower is capable of collecting more wind energy and producing a stronger vortex than a tower with a spiral cross-section. The estimated power outputs of Table 1 may be further increased with a multiple vaned tower. We have taken some data on such a tower. In order to present a complete picture, more data will be taken in the next contract phase. The combined data and their interpretation will be reported later.

3. FLOW ANALYSIS

A global or overall analysis is carried out for the Tornado-Type Wind Energy System. Mass, momentum, and angular momentum balance are performed on the tower, incorporating various parameters related to the inlet flow conditions, the flow state at the top exit of the tower, and the dimension of the viscous vortex core.

An important finding is that the tower may cause the incoming wind stream to accelerate before it enters the tower. Thus, the tower is capable of capturing energy from an area larger than its frontal area. This effect has a profound implication on the power output and has been observed in the laboratory. In addition, it is found that the power coefficient of the system improves strongly with the tower size or Reynolds number in agreement with our measured performance. Moreover, we obtain realistic results on the dependence of the power coefficient versus the turbine disk loading. Until now, previous attempts by others to predict the power coefficient have been either unrealistically overestimated or drastically underestimated as compared to present experimental data.

In spite of the simplicity of the global model, it yields the essential physics of the problem and, in addition, gives us further insight into the mechanics of the system. It should be reported that another extensive effort was made to solve the mean turbulent momentum equations using an integral method for the vortex structure and the system performance. The model used Mellor's (Ref. 14) generalized eddy viscosity for curved flows. The results we obtained, however, were highly sensitive to the shape of the assumed velocity profiles of the vortex. Major modifications of the model are needed before we can obtain reliable results which will be reported later.

The problem of modeling the fluid mechanics of the tornado-type wind turbine is inherently a difficult one. In the brief history of the device there have been a number of attempts by others to describe the physics of the problem. So (Ref. 15) used an infinite viscous vortex model that included axial flow to evaluate the performance of the mechanism. However, inherent in the analysis was the constraint that the tower diameter be much larger than

the turbine diameter, a restriction which clearly does not apply to the vortex tower. Hsu, Mellor, and Yen (Ref. 7) related the stagnation pressure drop due to viscous core to the change in pressure across the turbine and thus predicted the power output of the device. In another paper, Loth (Ref. 6) uses an ideal vortex model to predict a "Betz-type limit" for vortex wind machines. However, these descriptions though useful in some cases, were formulated utilizing grossly simplifying assumptions and consequently produced rather unrealistic conclusions. Moreover, unaccounted for in all these analyses was the effect of the tower height which is believed to be an important scaling parameter.

In order to successfully pursue the study of the dynamics of the vortex machine one needs a convenient and reasonably accurate scheme to model the overall important effects of the problem before solving the complete equations of motion. Hence, the intent in this study is to identify the critical physical parameters through an approach which looks at the global behavior of the mechanism. Consequently, the objective of this system analysis is to give us guidelines as to the performance rather than predicting the exact system behavior.

In this paper, mass, momentum, and angular momentum balances are carried out for a control volume encompassing the tower. These together with the radial momentum equation result in an algebraic system of two equations from which we are able to describe the inlet flow, internal fluid mechanics, and the flow condition at the top of the tower. Knowing the flow field pattern we then estimate the power coefficient as a function of disk loading.

The flow within the tower is taken to be axisymmetric. In this light, consider the flow system to be a cylinder of radius R and height H which is free of any torque as shown in Fig. 37.

DESCRIPTION OF INFLOW PARAMETERS

We first define the parameters α, β, and γ as denoted in Fig. 37. The product γV_∞ is the velocity at the inlet of the tower, γ is a dimensionless parameter indicating whether the flow at the inlet is accelerated or decelerated relative to the free stream velocity, V_∞; it signifies the shape of the inlet stream tube and delineates the size of the capture area. αV_∞ is the magnitude of the velocity at the cylindrical control surface $r = R$, where α is a dimensionless quantity. β is the angle between the velocity vector and the tangent direction at $r = R$.

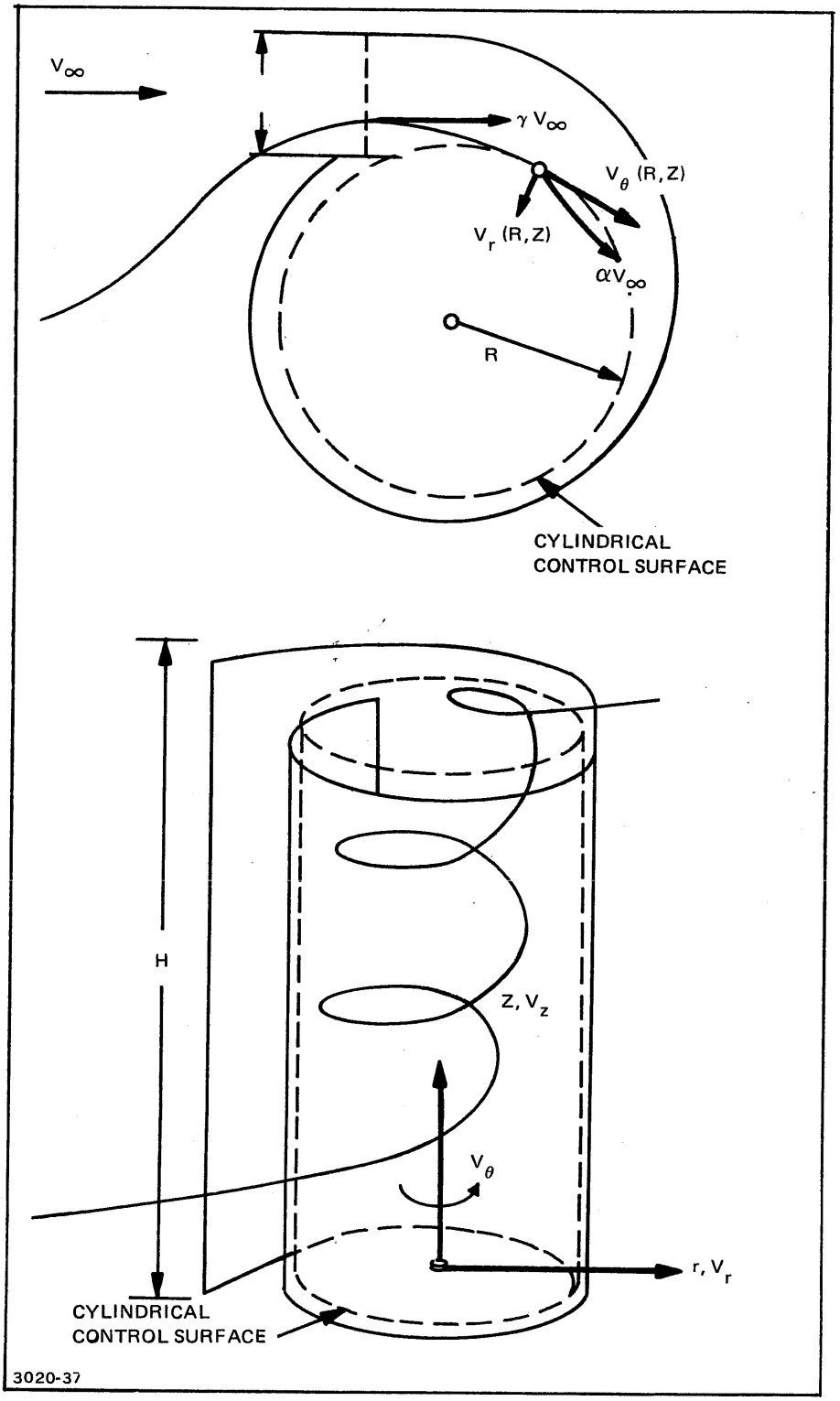

Fig. 37 Control Volumes and Nomenclature for Flow Analysis

Accordingly, the radial velocity component at r = R is

$$V_r(R,Z) = -\alpha V_\infty \sin\beta \tag{6a}$$

whereas the tangential velocity component at r = R is

$$V_\theta(R,Z) = \alpha V_\infty \cos\beta \tag{6b}$$

In general, α, β and γ are all functions of the space coordinate z, however for this study they will be considered to represent mean values and thus are treated as unknown constants which are to be determined.

BASIC EQUATIONS

By taking a control volume around the cylinder, conservation of mass for a steady incompressible flow is written as

$$\int_o^H \alpha V_\infty \sin\beta \; 2\pi R \, dz = \int_o^R 2\pi V_z(r,H) \, r dr - V_{Turb} \, \pi R_T^2 \tag{7}$$

where V_{Turb} denotes the velocity through the turbine.

If energy dissipation is negligible within the system we can then write Bernoulli's equation as

$$p_\infty + \rho \frac{V_\infty^2}{2} = p(r,H) + \frac{\rho}{2} \left. (V_\theta^2 + V_r^2 + V_z^2) \right|_{z = H} \tag{8}$$

where the left-hand side represents free stream conditions while the other side describes the state at z = H for all values of r. The pressure field at the top of the tower (the first term on right side of Eq. (8)) is

$$p(r,H) = p(R,H) - \rho \int_r^R \frac{V_\theta^2}{r} \, dr \tag{9}$$

where p(R,H) is the pressure at r = R and z = H and is considered a parameter of the problem. Further details concerning this quantity are given in subsequent discussions. Equation (9) is seen to be the radial momentum equation integrated from any r to r = R. It assumes the radial equilibrium of the centrifugal force with the inward pressure gradient force which is valid when the viscous effects are small. Rearranging Eq. (8) gives

$$V_z(r,H) = \sqrt{\frac{2}{\rho}(p_\infty - p(r,H)) + V_\infty^2 - V_\theta^2(r,H) - V_r^2(r,H)} \tag{10}$$

Around the same control volume one expresses the conservation of angular momentum as

$$\int_0^H \alpha^2 V_\infty^2 \sin\beta \cos\beta \, R^2 dz = \int_0^R V_z(r,H) \, V_\theta(r,H) \, r^2 dr \tag{11}$$

The approximation that $V_r(r,H) << V_\theta(r,H)$ is made since it is in agreement with our observations. It is seen that Eqs. (7), (10), and (11) contain three unknowns in α, β and $V_z(r,H)$ if $V_\theta(r,H)$ is specified.

Caution should be exercised in selecting the tangential velocity distribution at the top of the tower as it must contain the essential characteristics of a real vortex flow. In addition, it must satisfy the boundary conditions of this problem. Hence, we assume the profile

$$V_\theta = \frac{\alpha \cos \beta V_\infty R}{r} \left(1 - \exp(-r^2/\delta^2(H))\right) \tag{12}$$

where the viscous core radius at $z = H$ is denoted by $\delta(H)$. Note that for $r << \delta$, $V_\theta \sim r$ as in a solid body rotation and that for $r >> \delta$, $V_\theta \sim 1/r$ as in a potential vortex flow. For this problem the domain of δ is $0 \leq \delta \leq R$. It is seen from Eq. (12) that at

$$r = 0, \; V_\theta = 0 \tag{13a}$$

$$r = R, \; V_\theta \simeq \alpha V_\infty \cos \beta \tag{13b}$$

As will be shown later in this report, R^2/δ^2 is much greater than unity and as a result makes Eq. (13b) a good approximation as it must agree with Eq. (6b).

Since δ, in actuality, is an unknown quantity it will be considered to be a parameter of the problem. Therefore, α, β and $V_z(r,H)$ will be found for limiting values of δ. Thus, a map of all the possible values of α, β and $V_z(r,H)$ within these limits will be produced. These values are utilized next in calculating power coefficients and disk loadings which also define a performance map. This information is indispensible since it predicts the operating range and potential of the system.

As aforementioned, the pressure at the top of the tower is described by Eq. (9). Substituting the tangential velocity profile, Eq. (12) into the pressure relationship Eq. (4) gives

$$p(r,H) = p(R,H) - \rho \int_r^R \frac{\alpha^2 \cos^2 \beta V_\infty^2 R^2}{r^3} \left(1-\exp(-r^2/\delta^2)\right)^2 dr \tag{14}$$

Performing the integration yields two expressions in terms of exponential integrals for the pressure distribution, one being valid for $0 \leq r \leq \delta$ while the other being valid for $\delta \leq r \leq R$. The forms are given and described in the Appendix. The most important feature to note here is the dependence of $p(r,H)$ on the dimensionless viscous core, δ/R. The smaller the viscous core the larger the static pressure drop. Examining Eq. (12) shows that as the viscous core is made smaller the tangential velocity approaches a potential vortex ($V_\theta \sim 1/r$) and thus a larger pressure gradient is realizable.

The parameter $p(R,H)$ will be estimated to be the average azimuthal pressure at a solid circular cylinder produced by a flow around this cylinder. The justification for such an assessment are the flow visualization results of Figs. 9 and 10. They clearly show that the flow issuing from the top of the tower is a stable vortex with a nearly cylindrical surface. The average pressure coefficient, C_{P_H}, for flow around a solid cylinder with a Re = 6.7×10^5 is approximately -0.7 (Ref. 16)

$$C_{P_H} = \frac{p(R,H) - p_\infty}{\frac{1}{2}\rho V_\infty^2} \tag{15}$$

As Re approaches infinity the pressure coefficient approaches -1. For the vortex tower, typical Reynolds numbers are on the order of 10^6. Hence, one would expect the pressure coefficient to be somewhat larger in magnitude than -0.7. However, to obtain conservative estimates of the pressure at the location r = R and z = H the pressure coefficient will be taken to be significantly less than -0.7, for example, -0.5.

METHOD OF SOLUTION

Equations (7), (10), and (11) are a system of transcendental equations in α, β and $V_z(r,H)$. Equation (10) gives $V_z(r,H)$ as a function of α and β and hence substituting Eq. (10) into Eqs. (7) and (11) yields two equations in α and β only. Thus, the two equations to be solved are

$$\int_o^H \alpha V_\infty \sin\beta \, R dz = \int_o^R \sqrt{\frac{2}{\rho}(p_\infty - p(r,H)) + V_\infty^2 - V_\theta^2(r,H)} \, rdr - \frac{V_{Turb} R_T^2}{2} \tag{16}$$

and

$$\int_o^H \alpha V_\infty \sin\beta \, R dz = \int_o^R \sqrt{\frac{2}{\rho}(p_\infty - p(r,H)) + V_\infty^2 - V_o^2(r,H)} \, (1-\mathrm{Exp}(-r^2/\delta^2)) rdr \tag{17}$$

Substituting Eqs. (14) and (15) into Eqs. (16) and (17) yields

$$\alpha \sin\beta \, RH = \int_o^\delta \sqrt{(1-C_{P_H}) + F_1 \frac{R^2}{\delta^2} \alpha^2 \cos^2\beta} \, rdr$$

$$+ \int_\delta^R \sqrt{(1-C_{P_H}) + F_2 \frac{R^2}{\delta^2} \alpha^2 \cos^2\beta} \, rdr - \frac{1}{2} \frac{V_{Turb} R_T^2}{V_\infty} \tag{18}$$

and

$$\alpha \sin\beta RH = \int_o^\delta \sqrt{(1-C_{P_H}) + F_1 \frac{R^2}{\delta^2} \alpha^2 \cos^2\beta} \, (1-\exp(-r^2/\delta^2)) \, rdr$$

$$+ \int_\delta^R \sqrt{(1-C_{P_H}) + F_2 \frac{R^2}{\delta^2} \alpha^2 \cos^2\beta} \, (1-\exp(-r^2/\delta^2)) \, rdr \tag{19}$$

where F_1 and F_2 are given by Eqs. (A6) and (A7), respectively, of Appendix A.

These equations are easily solved for α and β using a standard numerical scheme. Results are given and discussed below.

RESULTS AND DISCUSSION

The objective of this investigation is to obtain general trends of how the vortex structure and the system performance change with various physical parameters of the problem. The results as presented and discussed below proved to be significant and encouraging.

Equations (18) and (19) are solved for α and β for certain values of the parameter δ/R. Figure 38 shows the expected variation of α with the dimensionless viscous core radius for a particular geometry and pressure coefficient, C_{P_H}. The inflow parameter is seen to decrease with increasing δ/R. This result can be explained with the aid of Fig. 39 which illustrates how α decreases with increasing β. Note that β is a small angle for most α values. Therefore, since it is the product $\alpha \cos\beta$ that appears in the tangential velocity component equation (Eq. (12)), one can conclude, from the above discussion, that larger α values signify larger tangential velocities since, $\cos\beta \simeq 1$. Therefore, increasing the value of α increases the local Reynolds number $V_\theta R/\eta$, or in other words the vortex strength, and hence diminishes the effects of viscosity which in turn necessitates a decreasing viscous core radius as shown in Fig. 38.

An extremely important and interesting finding is depicted in Fig. 40. It demonstrates how the critical factor γ, which indicates the size of the wind stream capture area, varies with α for given parameters. The parameter γ was found by assuming that all mass entering the inlet goes into the cylindrical control volume, i.e.,

$$\gamma V_\infty R_o H = \alpha V_\infty \pi D H \sin \beta \tag{20}$$

Rephrasing gives

$$\gamma = (\alpha \pi D/R_o) \sin \beta \tag{21}$$

This is a conservative estimate since all the fluid entering the tower will not, in reality, go into our imaginary control volume. It is clear that a γ value greater than unity indicates an accelerating flow which in turn signifies a converging incoming streamtube or a capture area larger than tower frontal area. In contrast, a bare turbine slows down the incoming wind stream, expands the streamtube, and as a result collects from an area smaller than its frontal area (Fig. 41). Any γ less than unity by the same token means a capture area less than the inlet area or a decelerating incoming flow. Figure 40 is based upon

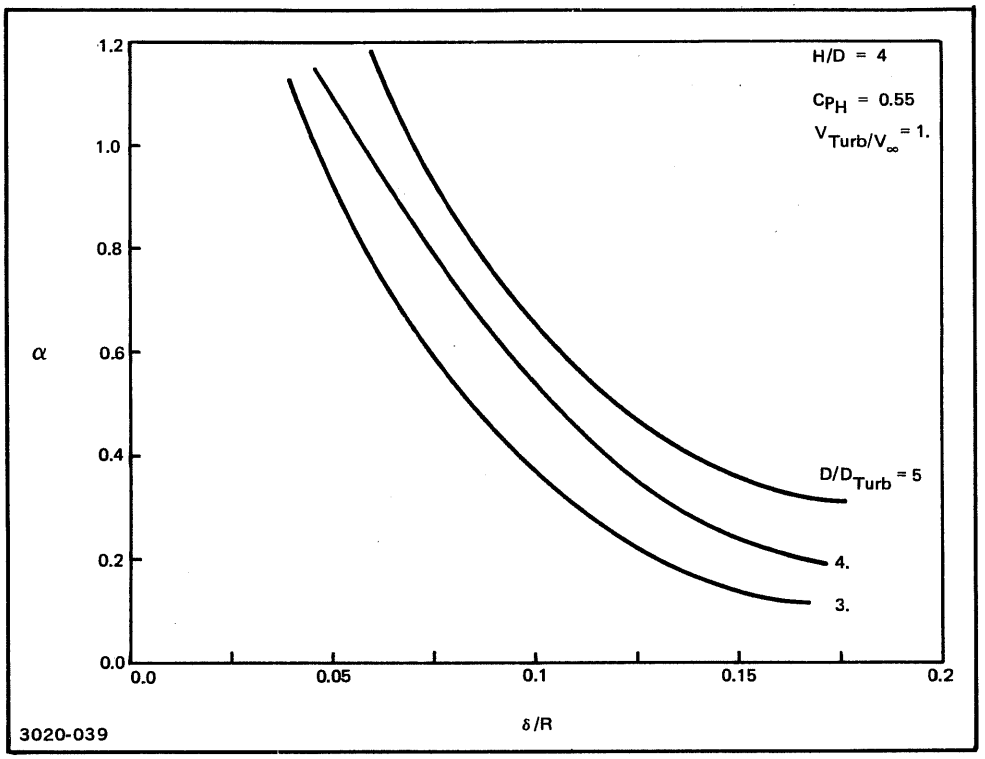

Fig. 38 Inlet Flow Parameter (Alpha) versus Dimensionless Viscous Core

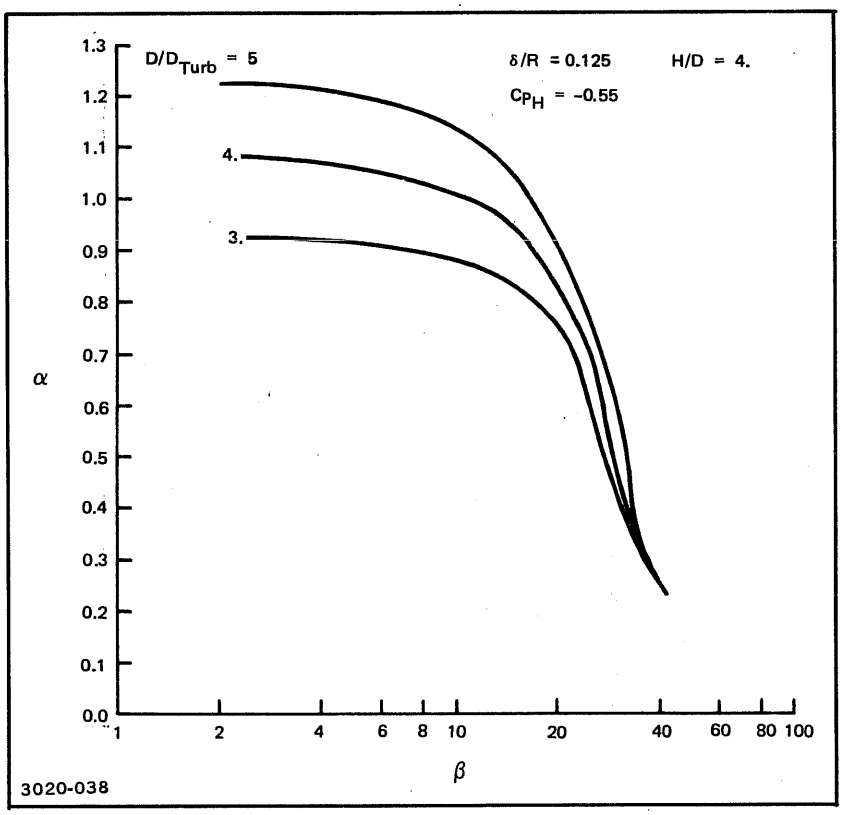

Fig. 39 Inlet Flow Parameter α vs Angle β

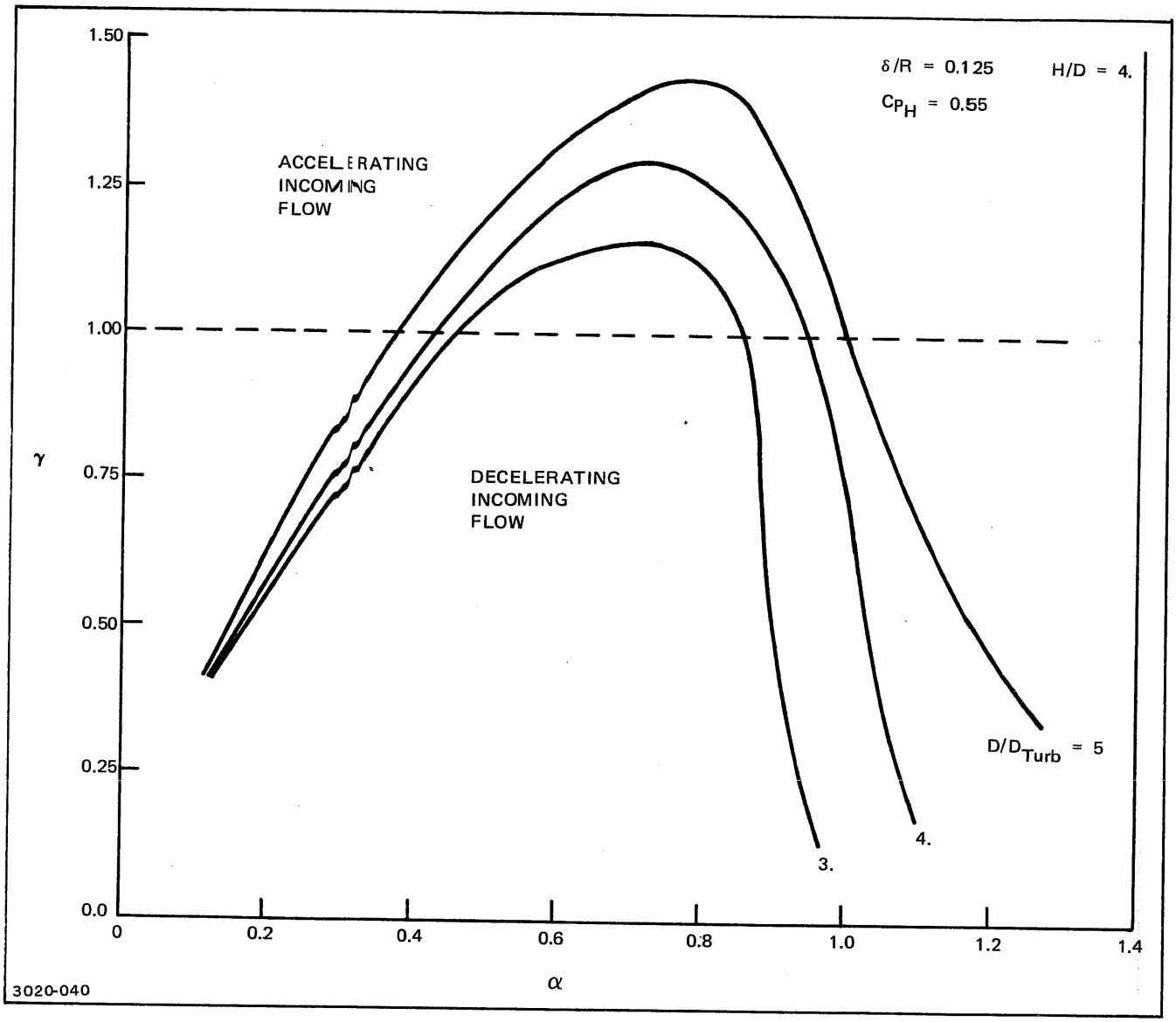

Fig. 40 Accelerating Factor γ vs Inflow Parameter α

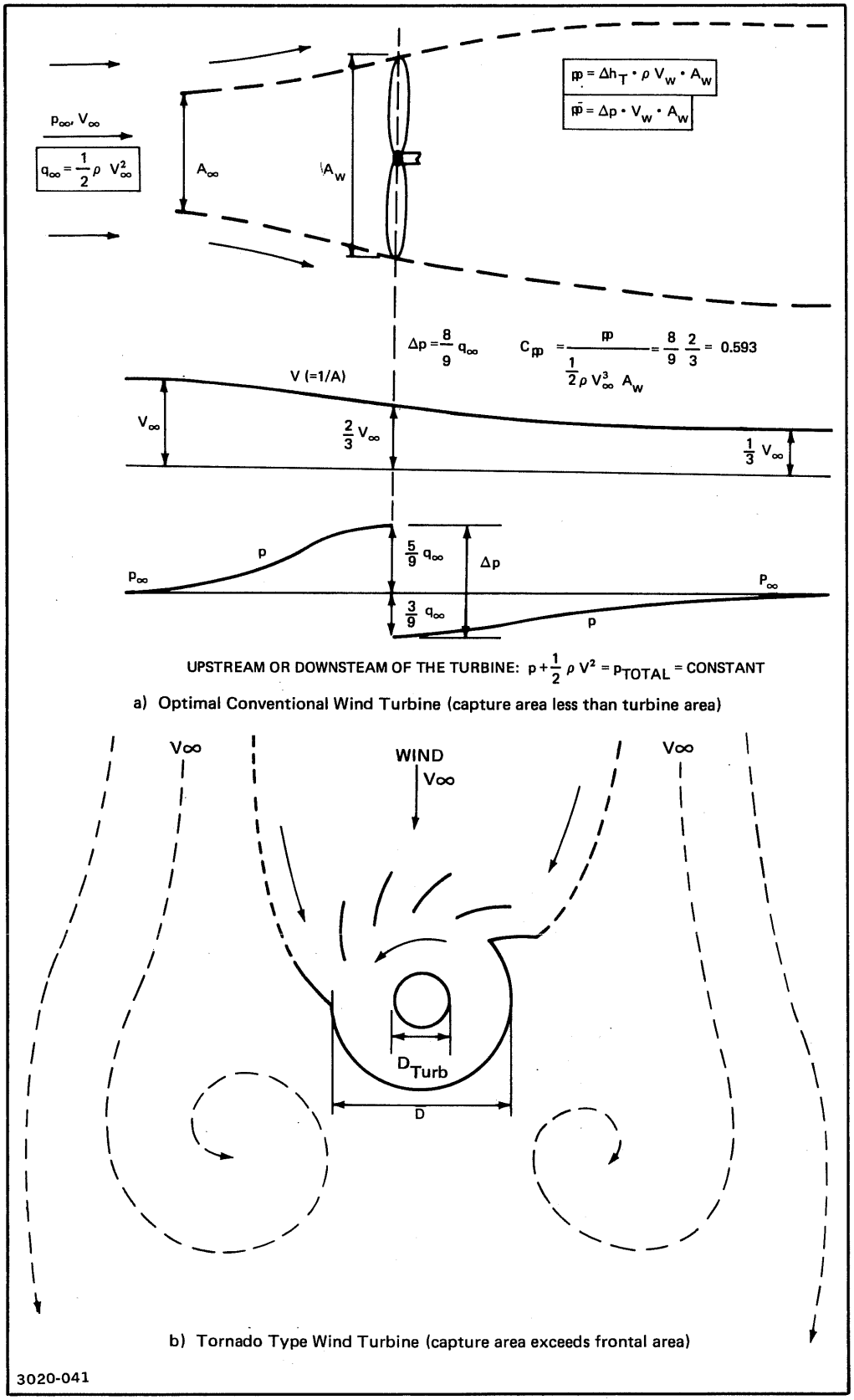

Fig. 41 Schematic Representation of Flow Field Around Wind Energy Machine

the ratio $D/R_o = 2.4$ and derived from the inforamtion given in Fig. 39. The simple but appealing conclusion is the fact that an analytical model actually predicts the possibility of an accelerating flow. Although this effect was shown experimentally it was never, until now, substantiated by theory.

The pressure distributuion at the bottom of the tower is obtained simply by assuming the radial equilibrium of the centrifugal force with the inward pressure gradient force. This is written as

$$p(r,o) = p(R,o) - \rho \int_r^R \frac{V_\theta^2}{r} \, dr \tag{22}$$

However, applying Bernoulli's equation from the free stream conditions to $r = R$ and $z = 0$ yields

$$p_\infty + \rho \frac{V_\infty^2}{2} = p(R,o) + \frac{\rho}{2} (\alpha V_\infty)^2 \tag{23}$$

Substituting Eq. (23) into Eq. (22) gives

$$p(r,o) = p_\infty + \rho \frac{V_\infty^2}{2} (1-\alpha^2) - \rho \int_r^R \frac{V_\theta^2}{r} \, dr \tag{24}$$

Therefore, we now have an expression which describes the pressure at the bottom of the tower as a function of r. Here it is assumed that the viscous core radius, $\delta(o)$, equal to value of the viscous core radius at the top of the tower, $\delta(H)$. In addition, the pressure over the turbine is taken to be the pressure at $r = R_I$, the turbine radius, as obtained from Eq. (24). In other words, the static pressure drops from $p(R,0)$ to $p(R_I,0)$ as illustrated in Fig. 42. The disk loading is defined to be

$$C_T = \frac{\Delta p_{Turb}}{\frac{1}{2} \rho V_{Turb}^2} = \frac{p_1 - p(R_1,0)}{\frac{1}{2} \rho V_{Turb}^2} \tag{25}$$

where p_1 is the static pressure immediately upstream of the turbine. However,

$$p_\infty + \rho \frac{V_\infty^2}{2} = p_1 + \rho \frac{V_{Turb}^2}{2} \tag{26}$$

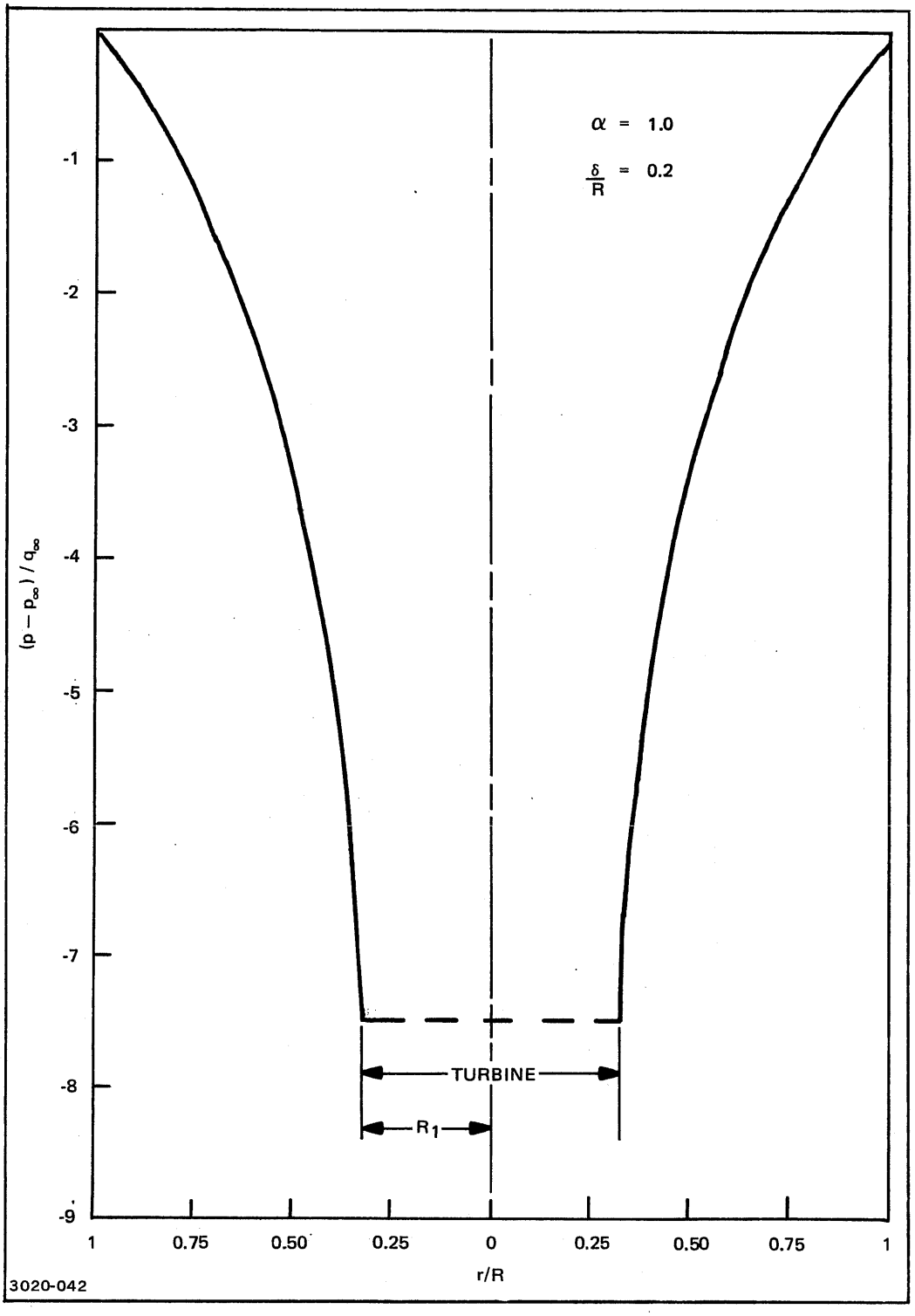

Fig. 42 Static Pressure Distribution at Tower Bottom

or rewritten

$$p_L = p_\infty + \frac{\rho}{2} \left(V_\infty^2 - V_{Turb}^2\right) \tag{27}$$

Substituting Eqs. (24) and (26) into Eq. (7) yields an expression for C_T as a funciton of V_{Turb}, α, β, H/D, D/D_{Turb} and C_{P_H} which are either knowns or parameters of the problem.

Furthermore, the power coefficient is defined by

$$C_P = \frac{\Delta p_{Turb}\ V_{Turb}\ A_{Turb}}{\frac{1}{2}\rho V_\infty^{\ 3}\ HD} \tag{28}$$

By the same substitutions one similarly obtains C_P as a function of V_{Turb}, α, β, H/D, D/D_{Turb} and C_{P_H}. The resultant expressions for C_P and C_T are given in the Appendix A.

A typical representation of the variation of the power coefficient C_P based on tower frontal area with the disk loadings C_T is demonstrated in Fig. 43. Here we compare the present theoretical results with our experimental data and as can be seen agree quite closely. The compatibility can only signify that the essential physics of the problem have been conserved by this global analysis despite its fundamental simplicity.

The figure describes a performance map for the vortex tower for values of δ/R between 0.1 and 0.18. That is to say, it provides a reasonable measure of the device's operational range. The lower bound of $\delta/R = 0.18$ was chosen since $\delta/R = 0.22$ produced fictitious negative values of C_P for this case. Note that the power coefficient increases as the viscous core radius decreases. As previously mentioned a smaller viscous core signifies higher local Reynolds numbers and hence lower static pressures immediately downstream of the turbine. This effect therefore indirectly confirms experimental measurements that exhibit increasing trends of C_P with Reynolds number. The upper bound of $\delta/R = 0.1$ was conservatively chosen to represent the best possible performance of the device. A value of $\delta/R = 0.1$ is achievable by simply increasing the free stream velocity and thus reduces the effect of viscosity. It is important to note that by roughly halving the viscous core from $\delta/R = 0.18$ to $\delta/R = 0.1$, the power coefficient is increased fourfold if the optimum disk loading is considered.

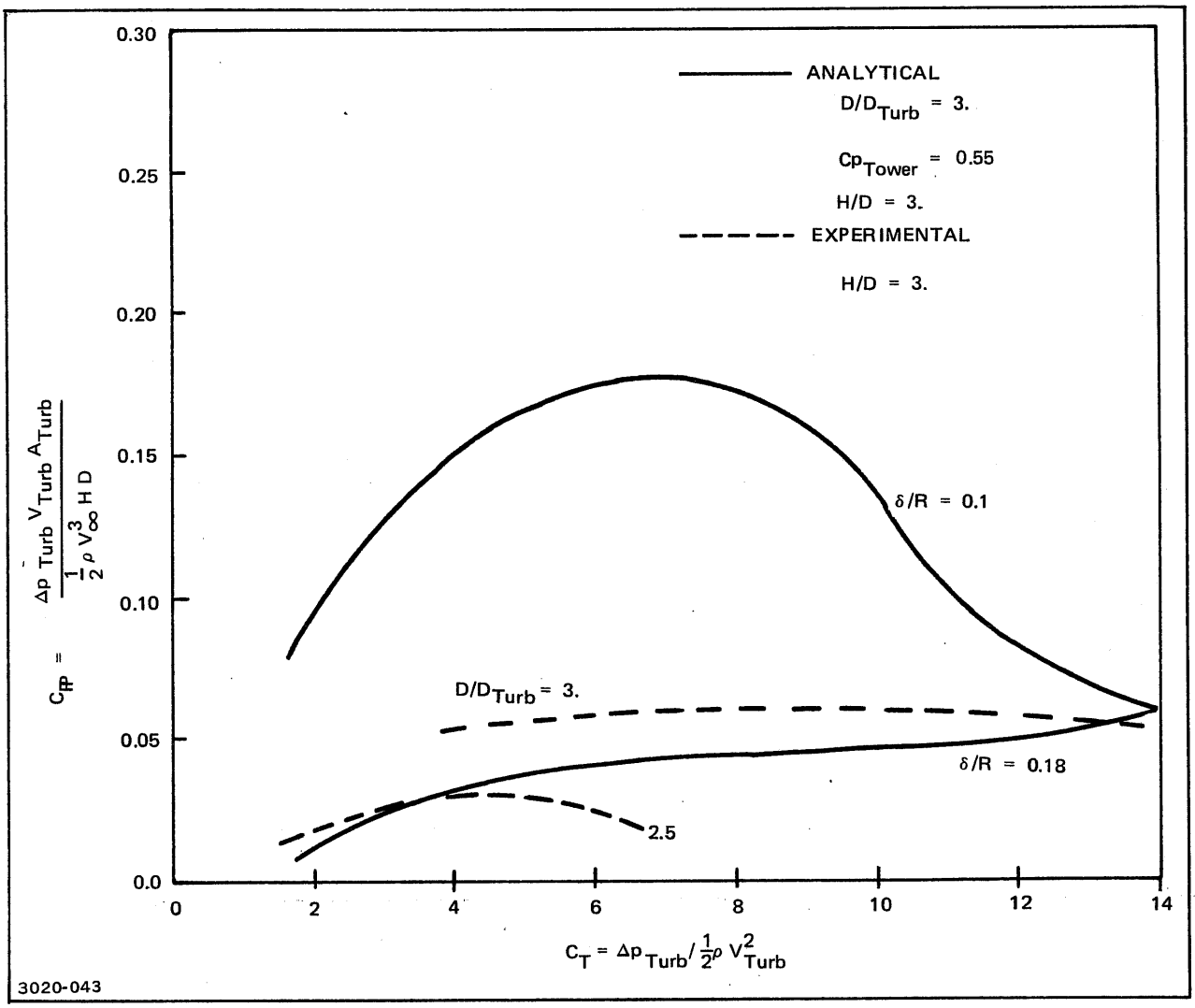

Fig. 43 Plot of Power Coefficient versus Disk Loading Coefficient and Comparison of Theory and Experiment

Therefore, in certain instances the power coefficient can vary as the inverse square of the viscous core. The importance of the viscous core radius cannot, as a result, be overemphasized.

Figure 44 depicts the effect of the aspect ratio H/D and diameter ratio D/D_{Turb} on the tower operation. Observe that increasing D/D_{Turb} increases the power coefficient which again confirms the experimental trends shown in Fig. 43. It is also important to note the increased performance due to a greater aspect ratio. This significant scaling effect has important ramifications with respect to the power output of the system and has been verified experimentally.

CONCLUSIONS

In conclusion, it is seen that the global analysis, though not complex, highlights the important mechanics of the problem. It confirmed the importance of the viscous core radius on the performance of the machine. In addition, it substantiated a favorable effect which was demonstrated experimentally, namely, the ability of the tower to capture from an area larger than its frontal area. Furthermore, it yielded realistic trends of C_P versus C_T. The method was also able to confirm other trends that were found in the laboratory which lends further credence to the theory. However, it must be realized that the complete problem remains unsolved. The global method served its intended purpose, that is, to identify the important physical factors of the problem and their general trends with other parameters. The absolute values of the parameters are really of no interest or importance. The method simply served to furnish us with guidelines as to the operation of the energy system.

Any further analytical work should take into account the important and complex bottom wall boundary layer-turbine flow interaction. In addition, the interaction of the free stream wind with the exiting vortex is of paramount importance and needs to be studied closely.

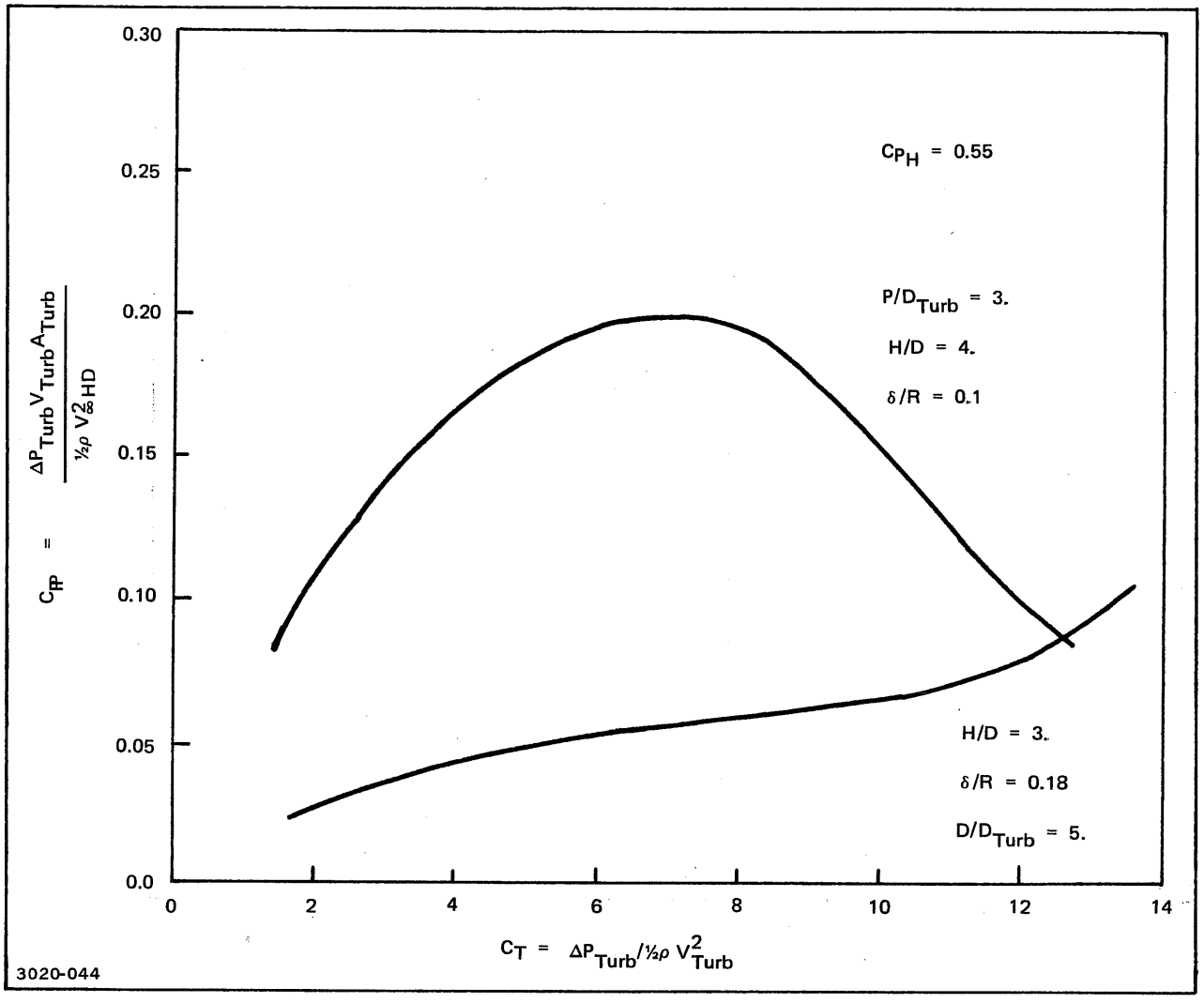

Fig. 44 Plot of Power Coefficient versus Disk Loading Coefficient for Various Values of D/D_{Turb}, H/D and δ/R

4. STRUCTURAL AND COST ANALYSIS

The object herein is to present a structural analysis of a variable thickness cylindrical tower for the Tornado-Type Wind Energy System. In what follows the stresses due to the wind loadings and due to the weight of the tower are first separately considered. Then, the superposition of these stresses gives the total stress due to both the wind and weight contributions. The superposition principle is valid since the deflecitons of the structure are small compared to the characteristic length (height for the tower). Figure 45 gives the nomenclature for this problem and depicts the superposition principle that is employed in this analysis. Another cost analysis using a different approach has been carried out in 1976 and is being issued as a separate Grumman memorandum (Ref. 17).

STRESSES DUE TO THE WEIGHT OF TOWER

The outer tower radius at $z = 0$ is denoted by R_o. The inner radius which is constant for all z is given by R_1. The object is to determine how the other radius $R(z)$ which is equal to the inner radius plus the thickness, $t(z)$, should vary with height in order that the compressive stress due to weight at all cross-sections should not exceed the allowable working stress of the tower material.

Let W denote the weight of that portion of the body of height z. Then dW represents the increment to W due to an increment of height dz. In addition, let A and A + dA be the corresponding areas. Considering the normal compressive stresses acting over both surfaces of this element, we have

$$\frac{W}{A} = \frac{W + dW}{A + dA} = \sigma_1 \tag{29}$$

But $dA = 2\pi RdR$ and $dW = \pi\gamma(R^2-R_1^2)$ where γ is the specific weight. Substituting these relations into Eq. (29) gives

$$\frac{2\pi RdR}{\pi\gamma(R^2-R_1^2)dz} = \frac{1}{\sigma_1} \tag{30}$$

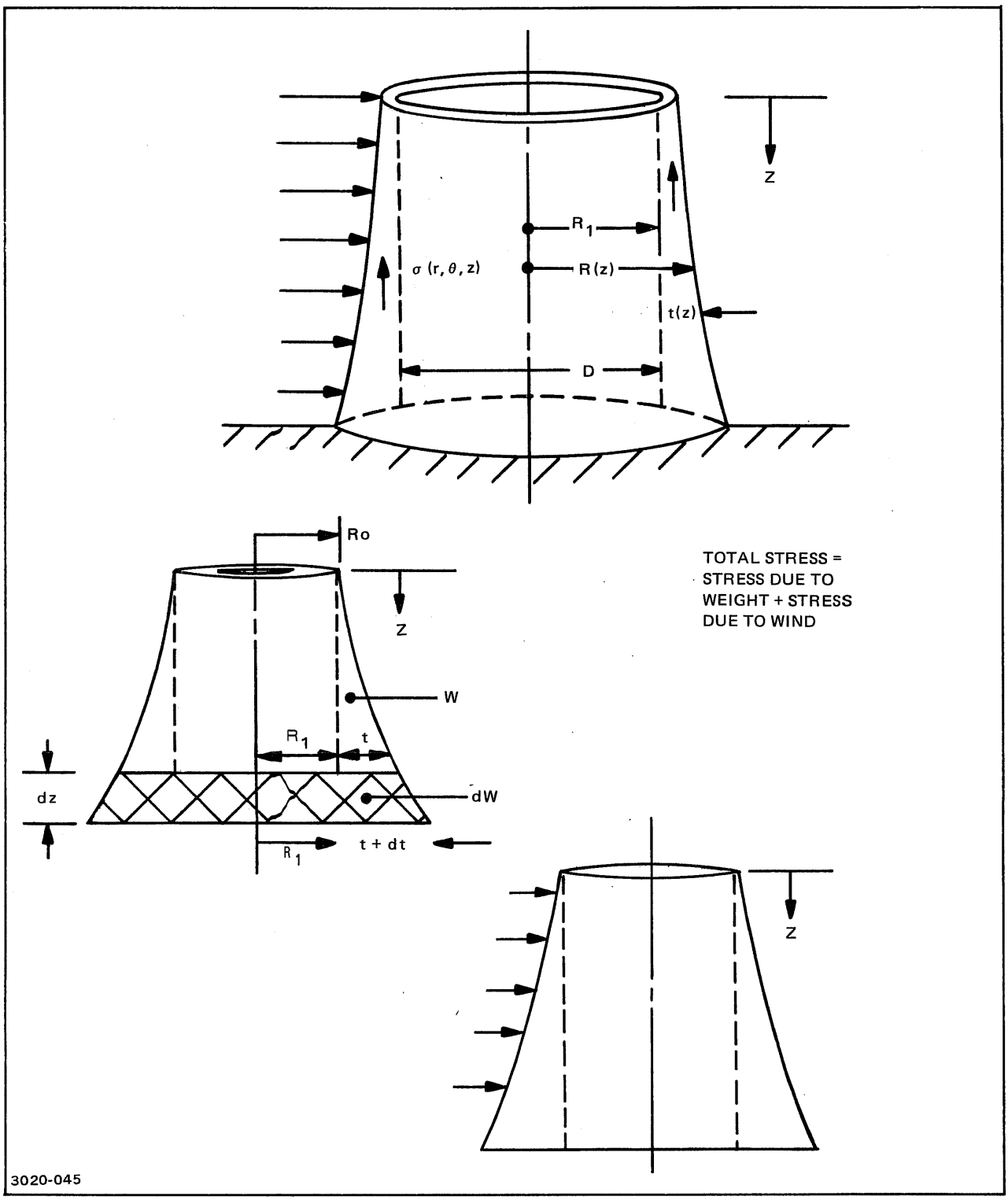

Fig. 45 Nomenclature for Structural Analysis

Integrating Eq. (30) with the initial condition that $R(0) = R_o$ yields

$$\sigma_1 = \frac{\gamma z}{2\ln\left[\frac{R^2-R_1^2}{R_o^2-R_1^2}\right]} \tag{31}$$

STRESSES DUE TO THE WIND

The aerodynamic wind loading on the tower is taken to be the azimuthal pressure distribution on a circular cylinder in a free stream. This is approximated by the piecewise functions

$$p(\theta) = \begin{cases} = q_\infty(1 - \frac{6}{\pi}\theta) & \text{FOR } 0 \leq \theta \leq \frac{\pi}{3} \quad (32a) \\ = -q_\infty & \text{FOR } \frac{\pi}{3} \leq \theta \leq \frac{5\pi}{3} \quad (32b) \\ = q_\infty(\frac{6}{\pi}\theta - 11) & \text{FOR } \frac{5\pi}{3} \leq \theta \leq 2\pi \quad (32c) \end{cases}$$

A typical pressure distribution is illustrated in Fig. 46. It is to be noted that this distribution gives the greatest pressure difference in the direction of the wind and hence produces the greatest moment. The external moment about the center of the tower in a direction parallel to the free streamlines is

$$M_{EXT} = \int_o^{2\pi} \int_o^{R_1} z\, p(\theta)\, R \cos\theta\, dR\, d\theta \tag{33}$$

Substituting Eqs. (32a), (32b), and (32c) into Eq. (33) gives

$$M_{EXT} = \frac{3}{2}\pi R_1^2 q_\infty Z \tag{34}$$

This external moment due to the wind must be balanced by the internal moment. Therefore, we have

$$M_{EXT} = \int_o^{2\pi} \int_{R_1}^{R_1+t} \sigma_2 R \cos\theta\, R\, dR\, d\theta \tag{35}$$

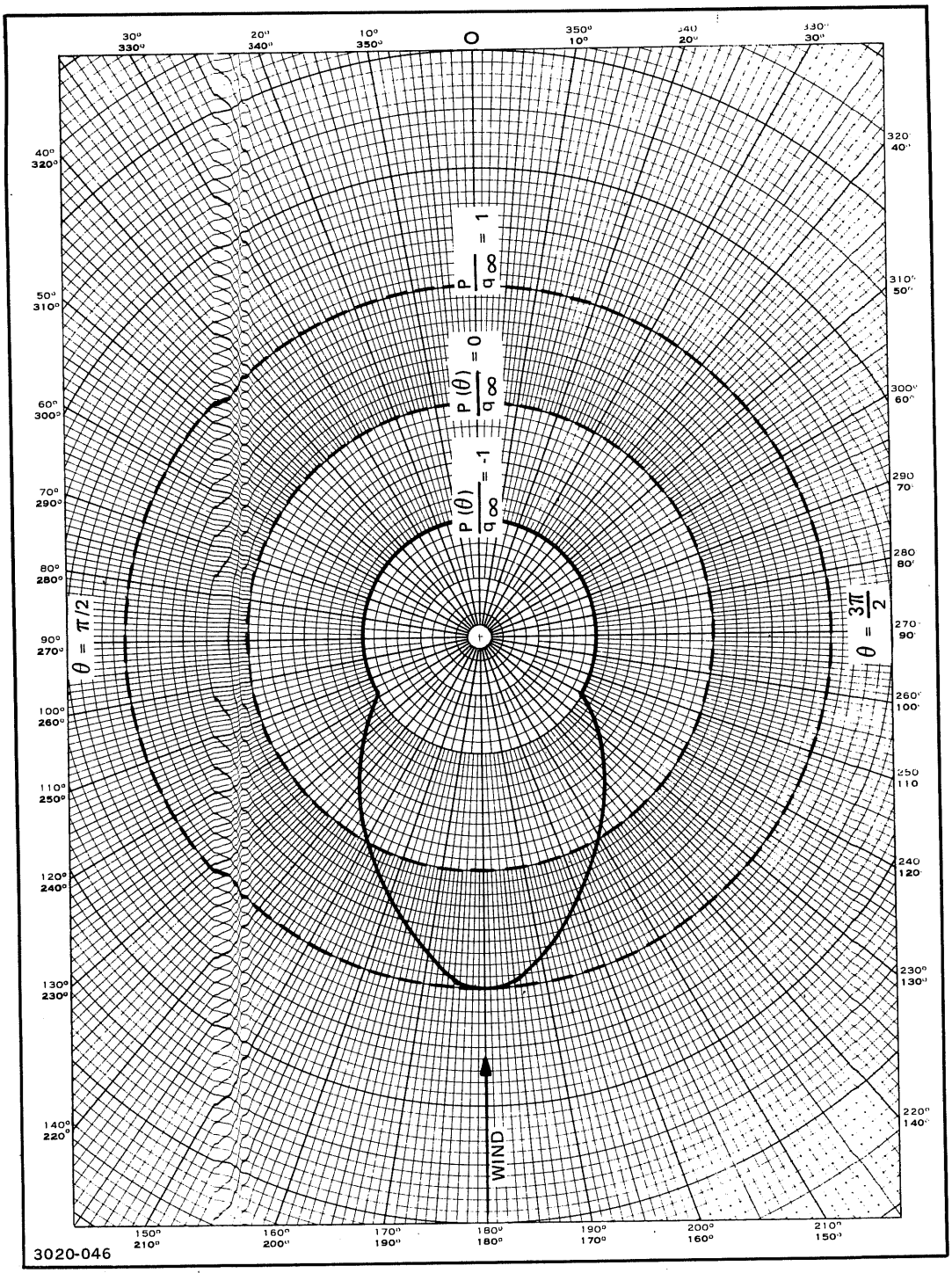

Fig. 46 Typical Pressure Distribution Around a Circular Cylinder (Ref. 16)

For a material which follows Hookes law, we have

$$\sigma_2 = E \frac{R}{R_c} \cos \theta \tag{36}$$

where E is the modulus of elasticity and R_c is the radius of curvature.

Combining Eqs. (35) and (36) and integrating yields

$$M_{EXT} = \frac{EI}{R_c} \tag{37}$$

where

$$I = \frac{\pi}{4} [R^4 - R_1^{\ 4}]$$

is the moment of inertia of the cross-section. Using Eqs. (34),(36),and (37) gives

$$\sigma_2 = \frac{6R_1^{\ 2} q_\infty z \ R \cos \theta}{(R^4 - R_1^{\ 4})} \tag{38}$$

TOTAL STRESS

Invoking the principle of superposition the total stress is simply the sum of the stress caused by the weight of the tower, Eq. (31), and the stress due to wind forces, Eq. (38), or

$$\sigma_T = \sigma_1 + \sigma_2$$

$$\sigma_T = Z \left[\frac{\gamma}{2 \ \ell n \left[\frac{R^2 - R_1^{\ 2}}{R_o^{\ 2} - R_1^{\ 2}} \right]} + \frac{6R_1^{\ 2} q_\infty R \cos \theta}{R^4 - R_1^{\ 4}} \right] \tag{39}$$

The total stress σ_T is set equal to one half the tensile strength. Therefore, after rearranging we have

$$Z = \frac{\sigma_w/2}{\left[\dfrac{\gamma}{2\,\ell n\left[\dfrac{R^2-R_1^2}{R_o^2-R_1^2}\right]} + \dfrac{6R_1^2 q_\infty R\cos\theta}{R^4-R_1^4}\right]} \tag{40}$$

Equation (40) gives an implicit expression for the tower outer radius R(z) as a function of the tower height z, measured from the top of the tower. The primary objective of this analysis, however, is to determine the specific material cost as a function of height for various wind loadings. Hence, if C denotes cost per pound of material, the average installed cost per square foot of tower wall area for a tower of height H is given by

$$\text{\$/unit of wall area (installed)} = \frac{5\gamma C\pi \int_o^H (R^2-R_1^2)\,dz}{\pi DH} \tag{41}$$

where a markup factor of 5 is used to get the installed cost from the raw material cost. Such a markup is recommended by Ref. 18 for products requiring an average amount of machinery and was used in Ref. 17.

Equation (41) is evaluated numerically since the outer radius isn't given as an explicit function of height z. Assuming a minimum thickness of 7.5 cm (3 in.) for concrete and 6mm (1/4 in.) for others, the required values for C, γ, σ_w and t_o are tabulated in Table 2.

TABLE 2 PROPERTY VALUES FOR VARIOUS MATERIALS

Material	¢($/lb)	γ $\frac{lb}{ft^3}$	σ_w(psi)	t_o(ft)
Concrete	0.02	144	625	0.25
Structural Steel	0.15	490	60,000	0.021
FRP	0.67	120	22,000	0.021
Aluminum Alloy	0.45	170	45,000	0.021
ABS	0.45	66	10,500	0.021

The resulting specific cost per tower wall area installed is plotted versus tower height for various maximum wind speeds in Figs. 47, 48, and 49. Note that for tower heights less than 300 m (1000 ft) the cost remains relatively constant, i.e., it is weakly dependent on the maximum wind speed. Also, ABS plastic, steel, or aluminum alloy are generally the cheaper materials to use. For H = 300 m (1000 Ft), these figures show that the specific tower cost is between \$140 to 160 per square meter (\$13 to 15 per square ft) of tower wall area installed for maximum wind speed of up to 72 m/s (160 mph).

We should emphasize that the above are conservative calculations since they assume free-standing towers made of solid walls and required to withstand the large bending moment at extreme wind speeds of up to 72m/s(160mph). Certainly, the tower can be anchored to the ground using guy wires or cables which will take up most of the bending moment. Then the stresses on and the cost of the tower walls can be greatly reduced.

The specific cost of the tower per rated kWe installed can be deduced from the above cost through the following relationship

$$\$/\text{KWe installed} = \frac{\pi \times \$/\text{wall area, installed}}{\frac{1}{2}\rho V_R^{\,3} \times F(H) \times C_P} \qquad (42)$$

where V_R is the rated wind speed at H_o = 9 m(30 Ft) and F(H) is a factor taking into account the increase in wind speed with height, up to the tower height H; F(H) is defined in Eq. (5) and for H = 300 m (1000 Ft), we have found that F(H) = 3.26, in Section 2 following the discussions in Table 1.

Taking the same basis as that for Table 1, namely, $C_P \sim R_e^{\,m}$ with m = 0.2 to 0.33, V_∞ = 11 m/s at 9 m (25 mph at 30 Ft), and H = 300 m (1000 Ft), Eq. (42) is evaluated and plotted in Fig. 50. For H = 300 m (1000 Ft), Figs. 47 to 49 have shown that the tower installed cost is between \$140 to 160/m^2 (\$13 to 15/ft^2) wall area as mentioned above. These values when combined with Fig. 50 give a specific tower cost of \$125 to 330/kWe installed as compared with the estimate of \$31 to 430/kWe installed given in Ref. 17. The latter estimate is reproduced as Tables 3 and 4 which are based on a rated wind speed of 13.4 m/s (30 mph). Thus, the upper bound for the specific tower cost has been lowered from the previous \$430/kWe installed to the new \$330/kWe installed. For a conservative estimation, we would still use the higher figure and put the upper bound of the

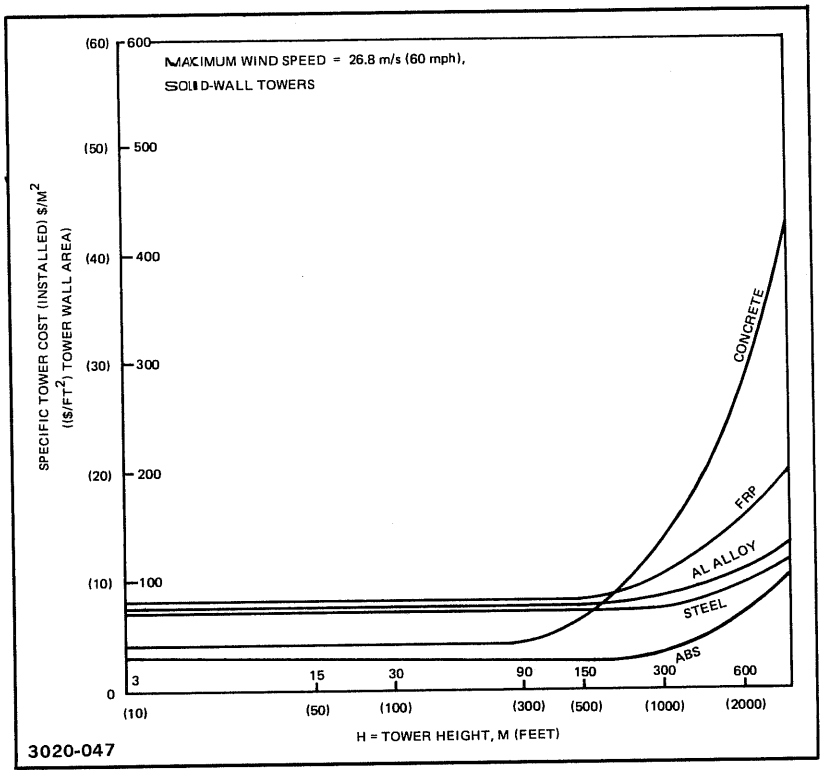

Fig. 47 Plot of Specific Tower Cost Installed versus Tower Height for Different Materials and with 26.8 m/s (60 mph) Maximum Wind Speed

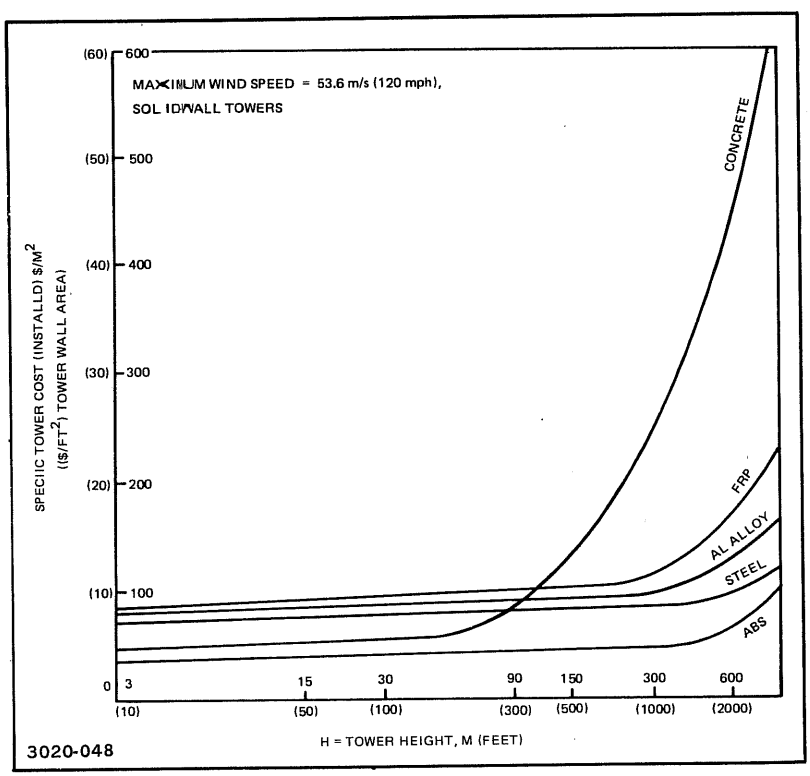

Fig. 48 Plot of Specific Tower Cost Installed versus Tower Height for Different Materials and with 53.6 m/s (120 mph) Maximum Wind Speed

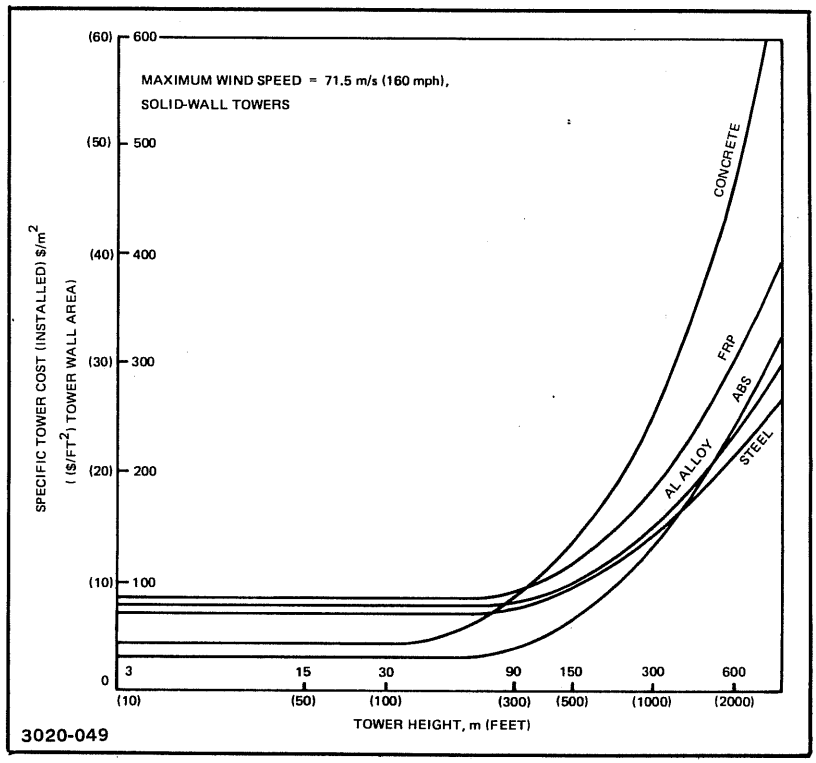

Fig. 49 Plot of Specific Tower Cost Installed versus Tower Height for Different Materials and with 71.5 m/s (160 mph) Maximum Wind Speed

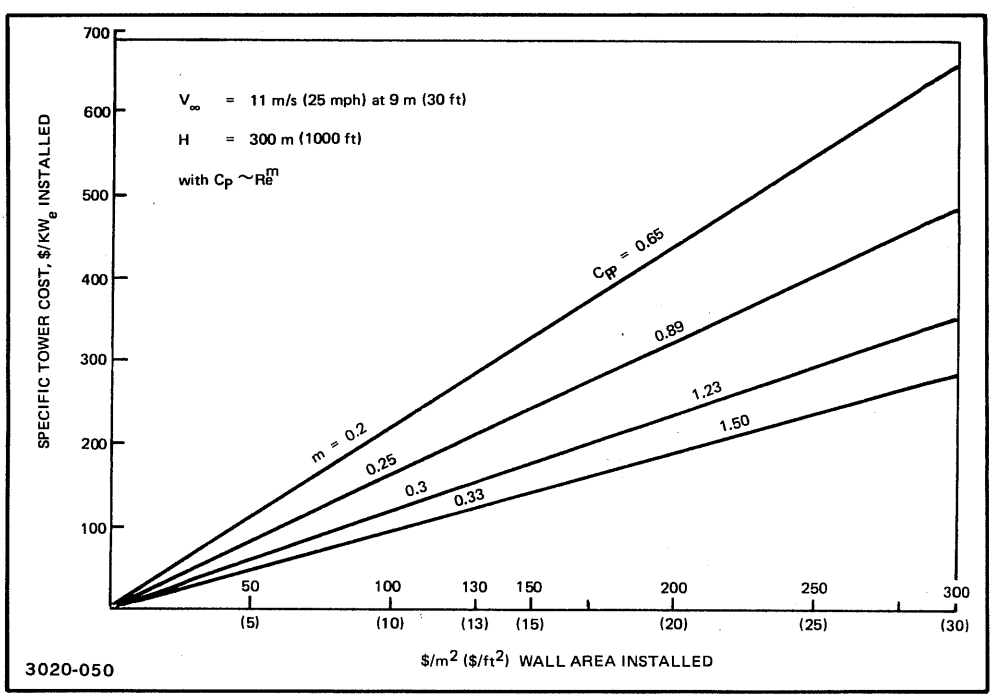

Fig. 50 Plot of Specific Tower Cost Installed versus Cost per Square Foot of Wall Area Installed for Different Scaling Laws and for a 300m (1000 Ft) Tower Height

TABLE 3 ESTIMATED COST ($/kW) OF CONVENTIONAL AND TORNADO-TYPE WIND ENERGY SYSTEMS UNDER MASS PRODUCTION (From Ref. 17)

	Conventional Systems		Tornado-Type Systems		
	100 kW System†	1 MW System††	1 MW System††	10 MW System††	100 MW System††
Rotor (Including Pitch-Control ($/ft^2 Turbine Area)	500 (4.3)	158 (6.3)	2-22 (63)	2-22 (63)	2-22 (63)
Mechanical Drive	325	162	2-22	2-22	2-22
Electrical Generator and Control	400	90	90	45	25
Tower	470	100	26-280†††	28-310†††	31-430†††
Installation	160	25	25	10	3
Site and Support Facilities	126	25	25	10	3
Total, per kW	$1,980	$560	$170-465	$100-420	$65-505

† Rated at 18 mph
†† Rated at 30 mph
†††For an aluminum tower

TABLE 4 COMPARISON OF ELECTRICITY BUSBAR COSTS BASED ON TABLE 3 (From Ref. 17)

	Conventional Systems		Tornado-Type Systems		
	100 kW System	1 MW System	1 MW System	10 MW System	100 MW System
Carrying Charge ($/kW)	300	84	26-70	15-63	10-76
Plant Factor	0.37	0.35	0.35	0.35	0.35
Cost per kW hr	9.5	2.9	1.1-2.5	0.7-2.3	0.5-2.7

estimated specific system cost at \$505/kWe installed and the upper bound of the estimated energy cost at 2.7 cents/kWh, as given in Tables 3 and 4. In comparison, the first units of Mod-OA propeller turbine cost \$6260/kWe installed (\$1.252 million for 200 kWe rated) with an energy cost ranging from 20 to 36 cents/kWh as reported in Ref. 10. With a usual "90% learning curve", these costs may be reduced by a factor of around three when the turbine system is mass produced. The Mod-1 turbine at mass production is estimated (Ref. 11) to have a capital cost of \$1650/kWe installed and an energy cost of 8.1 cents/kWh.

Finally, we may compare our estimated tower cost with the reported (Ref. 19) costs of the solar tower, the vital statistics of which are listed below.

- Rated capacity: 100 mWe
- Capacity factor = 37%
- Annual output = 320×10^6 kWh
- Operational life = 30 years
- No. of heliostats = 15,000
- Reflection area/heliostat = 331 ft^2
- Total mirror area = 5×10^6 ft^2
- Number of towers = 2
- Height of tower = 750 ft
- Total land area = 27×10^6 ft^2
- Capital cost at mass production = \$860/kWe installed

The system capital cost, the rated capacity, and the total mirror area are combined to yield a specific system cost of \$183/m^2 (\$17/ft^2) of mirror surface area installed, compared with our estimated specific tower cost of \$140 to 160/m^2 (\$13 to 15/ft^2) of tower area installed. Their cost includes not only the mirrors but also the control system, the tower and boiler, the electrical generator and, the mirror supports. Our cost includes only the tower, the control system for the vanes, and the supports for the tower. Moreover, the cost per square meter of the mirrors should be much higher than that of our tower surface. Hence, it seems that our estimated specific tower cost is a conservative estimate.

5. REFERENCES

1. Yen, J.T., "Tornado-Type Wind Energy System," Proceedings, Intersociety Energy Conversion Engineering Conference, September 1975, pp. 987-994.

2. Yen, J.T., "Tornado-Type Wind Energy System, Basic Considerations," ASME Paper 76-WA-Ener-2, 1976.

3. Yen, J.T., Summary of Recent Progress on Tornado-Type Wind Energy Systems, Third Wind Energy Workshop, ed. J.B.F. Scientific Corp., Washington, D.C., September 1977, pp. 808-818.

4. Yen, J.T., "Tornado-Type Wind Energy System - Semiannual Status Report," Grumman Research Department Memoranudm RM-643, September 1977.

5. Lewellen, W.S., "A Review of Confined Vortex Flows," NASA CR-1772, 1971.

6. Loth, J.L., "Betz Type Limitation of Vortex Wind Machines," Wind Engineering, Vol. 1, 1977, pp. 186-197.

7. Hsu, C.T., Mellor, G. and Yen, J.T., "Some Flow Analysis of a Tornado-Type Wind Turbine," to be presented at ASME Winter Annual Meeting, December 1978.

8. Glauert, H., "The Elements of Airfoil and Airscrew Theory," Cambridge University Press, 1943, pp. 222-226.

9. Igra, O., "Design and Performance Characteristics of a Shrouded Aero-generator Turbine," University of the Negev Report, 1974.

10. Robbins, W.H. and Sholes, J.E., "ERDA/NASA 200 kW Mod-OA Wind Turbine Program," Third Wind Energy Workshop, September 1977, Washington, D.C., Vol. 1, pp. 59-75.

11. Barchet, R.J., "Mod-1 Wind Turbine Generator Program," Third Wind Energy Workshop, September 1977, Washington, D.C. Vol. 1, pp. 76-91.

12. Sisterson, D.L. and Frenzen, P., "Nocturnal Boundary-Layer Wind Maxima and the Problem of Wind Power Assessment," Argonne National Laboratory Report, 1978.

13. von Karman, T., Zeit f. Angew, Math. Mech., Vol. 1, 1921, p. 239.

14. Mellor, G.L., "A Comparative Study of Curved Flow and Density Stratified Flow," J. Atmos. Sci., Vol. 32, 1975, pp. 1287-1292.

15. So, R.M.C., Paper presented at the ASME Spring Meeting, Atlanta, Ga., 1978.

16. Schlicting, H., "Boundary Layer Theory," McGraw Hill Book Co., N.Y. 1955.

17. "A Cost Analysis for Tornado-Type Wind Energy Systems," originally prepared as part of a 1976 Grumman proposal to U.S. Department of Energy, and to be issued as a Grumman Research Memorandum.

18. Machine Design, pp. 50-53, August 1975, in particular, see p. 53.

19. Bennington, G. et al, "Solar Energy: A Comparative Analysis to the Year 2020," Tech. Rept. MTR-7579, Mitre Corp., Metrek Division, McLean, VA., 1978.

ACKNOWLEDGEMENT

The author would like to acknowledge with appreciation the important contributions of S. Torquato who carried out the Flow and the Cost Analyses and wrote Sections 3 and 4. He would also like to express his appreciation to R. Oman for overall guidance and many useful discussions and suggestions, to K. Foreman for many helpful suggestions, to B. Gilbert for useful assistance in instrumentation, to W. Zyman for his outstanding craftsmanship and zealous assistance, and to J. DeCarlo for his substantial assistance.

APPENDIX A

The integration performed in Eq. (14) is given and described below. Hence, from Eq. (14) we let

$$\tilde{F} = \rho\ V_\infty{}^2 R^2 \alpha^2 \cos^2\beta \int_r^R \frac{(1-e^{-r^2/\delta^2})}{r^3}\, dr \tag{A1}$$

Preforming the integration gives us

$$\tilde{F} = \frac{\rho V_\infty{}^2 R^2\ {}^2\cos^2\beta}{2\delta^2}\left[\frac{-(1-e^{-u})^2}{u}\Bigg|_u^K + 2(E_1(K)-E_1(u)+E_1(2u)-E_1(2K))\right] \tag{A2}$$

where E_1 is the exponential integral defined to be

$$E_1(Z) = \int_z^\infty \frac{e^{-t}}{t}\, dt$$

and

$$u = r^2/\delta^2 \quad ; \quad K = R^2/\delta^2$$

Equation (A2) can be put in the form

$$\tilde{F} = \frac{\rho V_\infty{}^2 R^2 \alpha^2 \cos\beta}{2\delta^2}\left[F_A + \frac{(1-e^{-u})^2}{u}\right] \tag{A3}$$

where

$$F_A = \frac{-(1-e^{-K})^2}{K} + 2(E_1(K)-E_1(u)+E(2u)-E(2K))$$

It is to be noted that the term $\rho V_\infty{}^2 R^2 \alpha^2 \cos^2\beta (1-e^{-u})^2/\delta^2 u$ in Eq. (A3) is in fact the tangential velocity squared. Substituting Eqs. (A1) and (15) into Eq. (14) gives

$$p(r,H) = \frac{1}{2}\rho V_\infty^2 C_{P_H} + p_\infty - F$$

$$p(r,H) = \frac{1}{2}\rho V_\infty^2 + p_\infty - \rho V_\infty^2 R^2 \alpha^2 \cos^2\beta F_A - \frac{\rho V_\theta^2}{2} \tag{A4}$$

Now substituting Eq. (A4) into Eq. (10) yields

$$V_z(r,H) = \sqrt{V_\infty^2(1-C_{P_H}) + \frac{\rho V_\infty^2 R^2 \alpha^2 \cos^2\beta}{2\delta^2} F_A} \tag{A5}$$

where we have used the approximation that $V_r(r,H) << V_\theta(r,H)$. The exponential integrals contained in F_A can be expressed as polynomials with a specified range of validity. Therefore, F_A is divided up into two parts, one portion, F_1, valid for $o \leq r \leq \delta$ and the other, F_2, valid for $\delta \leq r \leq R$. F_1 is found to be

$$F_1 = \left\{ \frac{-(1-e^{-K})^2}{K} + 2 \sum_{n=o}^{5} a_n u^n (1-2^n) + 2\,\ell n 2 - \frac{e^{-2K}}{K}\left[\frac{4K^2+4b_3K+b_4}{4K^2+2b_1K+b_2}\right] + \frac{2e^{-K}}{K}\left[\frac{K^2+b_3K+b_4}{K^2+b_1K+b_2}\right]\right\} \tag{A6}$$

whereas

$$F_2 = \left\{ \frac{-(1-e^{-K})^2}{K} - \frac{e^{-2K}}{K}\left[\frac{4K^2+2b_3K+b_4}{4K^2+2b_1K+b_2}\right] + \frac{2e^{-K}}{K}\left[\frac{K^2+b_3K+b_4}{K^2+b_1K+b_2}\right] - \frac{2e^{-u}}{u}\left[\frac{u^2+b_3u+b_4}{u^2+b_1u+b_2}\right] + \frac{e^{-2u}}{u}\left[\frac{4u^2+2b_3u+b_4}{4u^2+2b_1u+b_2}\right]\right\} \tag{A7}$$

The constants a_i and b_i are given on p. 231, Handbook of Mathematical Functions, published by National Bureau of Standards, with Eqs. (A6) and (A7) we are able to obtain the two final Eqs. (18) and (19).

Let us now consider the expressions for $C_{\mathbb{P}}$ and C_T. The pressure drop across the turbine is

$$\Delta p_{Turb} = p_1 - p(R_1,0) \tag{A8}$$

but from Eq. (24)

$$p(R_1,0) = p_\infty + \rho\frac{V_\infty^2}{2}(1-\alpha^2) - \rho\int_r^R \frac{V_\theta^2}{r}\,dr \tag{A9}$$

Substituting Eq. (A1) into (A9) gives

$$p(R_1,0) = p_\infty + \rho\frac{V_\infty^2}{2}(1-\alpha^2) - \rho\tilde{F} \tag{A10}$$

Eq. (A10) together with Eq. (26) yields

$$\Delta p_{Turb} = \frac{\rho}{2}\left[V_\infty^2\alpha^2 - V_{Turb}^2\right] + \rho\tilde{F}$$

Therefore, according to the definition given in Eq. (25)

$$C_T = \frac{V_\infty^2}{V_{Turb}^2}\alpha^2 - 1 + \frac{2\tilde{F}}{V_{Turb}^2} \tag{A11}$$

and according to definition given in Eq. (28)

$$C_{\mathbb{P}} = \frac{V_{Turb}\,\pi D}{V_\infty^3\,4H}\left[(V_\infty^2\alpha^2 - V_{Turb}^2) + 2\tilde{F}\right] \tag{A12}$$